Heavy-lepton interpretation of multimuon events produced in neutrino and antineutrino beams*

Carl H. Albright
Department of Physics, Northern Illinois University, DeKalb, Illinois 60115 †
and Fermi National Accelerator Laboratory, Batavia, Illinois 60510

J. Smith and J. A. M. Vermaseren
Institute for Theoretical Physics, State University of New York at Stony Brook, Stony Brook, New York 11794
(Received 9 May 1977)

We calculate neutrino production of a charged heavy lepton M^- from an isoscalar target assuming both light-to-light and light-to-heavy quark transitions. Then we examine the cascade decay of the M^- into another heavy lepton L^0 via $M^- \to L^0 + X$ and $M^- \to L^0 + \mu^- + \bar{\nu}_\mu$, followed by the decay of the L^0 into both $\mu^- + X$ and $\mu^- + \mu^+ + \nu_\mu$. These decays yield $\mu^-\mu^-$, $\mu^-\mu^+$, and $\mu^-\mu^-\mu^+$ multimuon events. We compute event rates and distributions for these types of lepton cascade chains. Also, we discuss results for the antineutrino production of the M^+ followed by analogous decay chains resulting in $\mu^+\mu^+$, $\mu^+\mu^-$, and $\mu^+\mu^+\mu^-$ events.

I. INTRODUCTION

The existence of heavy leptons[1] is an ingredient in many of the gauge-field models proposed to unify weak and electromagnetic interactions. Searches for such particles have been made in e^+e^- storage rings and in neutrino interactions. A charged heavy lepton, now called the τ, has been found by Perl *et al.*[2] in experiments performed at the colliding electron-positron beam facility SPEAR. Recent results from the colliding ring DORIS[3] are in good agreement with the SPEAR data. Thus it seems that the search for a new charged heavy lepton has been successful.

Neutrino experiments performed prior to 1976 were inconclusive with regard to finding heavy leptons. In particular, only a lower limit could be placed on the mass of a positively charged heavy lepton[4] coupling to ν_μ. Also, the bulk of the dimuon events[5] seen in neutrino experiments at Fermilab have the wrong characteristics to be associated with the decay products of a neutral heavy lepton.[6] In particular, the energy asymmetry between the μ^- and the μ^+ rules out a low-mass L^0 coupling with full strength to ν_μ via a neutral current.

The discovery of trimuon events,[7] together with the recent surge of interest in gauge models[8] incorporating the decay $\mu \to e\gamma$, has removed many inhibitions about the existence of several new charged and neutral leptons. The trimuon events easily fit the characteristics expected from a heavy-lepton cascade decay.[9,10] However, the event rate is so large that the new leptons probably have to be assigned to a gauge group larger than $SU(2) \times U(1)$.[9] In fact some $SU(3) \times U(1)$ gauge theory models have already been proposed which include new leptons as the source of the dimuon and trimuon events.[11] While it is too early to know which gauge model, if any, can fit the data, it is appropriate to undertake a thorough phenomenological analysis of a typical cascade decay chain. One alternative explanation of the trimuon events, namely, that they are the decay products of charmed particles produced from valence and sea quarks, does not give a good fit to the data.[12] The possibility still arises that the trimuon events could be the decay products of diffractively produced charmed particles[13] and more work is necessary to distinguish between this model and the heavy-lepton cascade decay model.

In this article we assume the existence of two spin-$\frac{1}{2}$ heavy leptons which we call M^- and L^0. For the most part we assume the M^- to have a mass equal to 8 GeV/c^2 and a charged-current coupling to the ν_μ-μ^-. The two-step decay of the M^- into the L^0 and then the L^0 into leptons and hadrons gives dimuon and trimuon final states. We postulate that all couplings are of charged-current vector or axial-vector type. Clearly, the addition of neutral currents is possible and would lead to many additional decays. These possibilities should be examined when more data becomes available. With the L^0 mass equal to 4 GeV/c^2, it can decay into the τ particle but we do not consider this possibility here. We have examined a range of values for the mass of the L^0. Hence our model assumes the M^- is produced initially via the reaction,

$$\nu_\mu + N \to M^- + X, \tag{1.1}$$

shown in Fig. 1. Many authors[14] have already

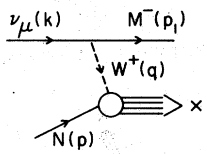

FIG. 1. Feynman diagram for the production of the heavy lepton M^- in neutrino interactions off isoscalar targets.

studied this process assuming quark-parton-model structure functions. We extend the previous analysis to include M^- production off light quarks leading to either light, charmed, or heavy quarks. If we then allow the M^- to decay via the usual mode $M^- \to \mu^- + \bar{\nu}_\mu + \nu_\mu$, the reaction gives single-μ^- events which are exceedingly difficult to extract from the regular process $\nu_\mu + N \to \mu^- + X$. Our preferred decays are therefore $M^- \to L^0 + X$ and $M^- \to L^0 + \mu^- + \bar{\nu}_\mu$ followed by the decays $L^0 \to \mu^- + X$ and $L^0 \to \mu^- + \mu^+ + \nu_\mu$. Thus our decay chains lead to the following reactions:

$$M^- \to L^0 + X$$
$$\searrow \mu^- + \mu^+ + \nu_\mu \qquad (1.2)$$

depicted in Fig. 2,

$$M^- \to L^0 + \mu^- + \bar{\nu}_\mu$$
$$\searrow \mu^- + X \qquad (1.3)$$

depicted in Fig. 3, and

$$M^- \to L^0 + \mu^- + \bar{\nu}_\mu$$
$$\searrow \mu^- + \mu^+ + \nu_\mu \qquad (1.4)$$

depicted in Fig. 4. These decay chains lead to neutrino-induced multimuon events with $\mu^-\mu^+$, $\mu^-\mu^-$, and $\mu^-\mu^-\mu^+$, respectively. Similar chains lead to antineutrino induced $\mu^+\mu^-$, $\mu^+\mu^+$, and $\mu^+\mu^+\mu^-$ events. Using only charged-current couplings avoids a potential problem associated with a high rate for L^0 production at the initial vertex, and hence the production of too many opposite-sign dimuon events.[6]

We concentrate on the decay modes which lead to final states involving muons. There are many variations of M^- and L^0 decays leading to electrons and positrons but we prefer to discuss them separately. Bubble-chamber experiments should be able to identify such decay modes. In fact, our model predicts a large decay rate into such channels. We fold our production cross sections with the neutrino flux for the quadrupole-triplet-target train used by the Fermilab-Harvard-Pennsylvania-Rutgers-Wisconsin (FHPRW) group. This means that it is difficult to extrapolate our results to other experiments. Clearly, the production of a very heavy lepton is extremely sensitive to the high-energy tail of the neutrino and antineutrino spectra. Event rates for experiments using dichromatic beams can be very different from those measured by the FHPRW group. However, the decay distributions are relatively insensitive to the production cross section, so we can predict with reasonable accuracy the key features expected from the cascade chain. Note that we do not try to compare our results with the currently available data sample since the number of events observed is very small, and the detection efficiency, acceptance, and resolution of the experimental apparatus is not yet known. There should be many more dimuon and trimuon events analyzed in the next few months both at Fermilab and at CERN.

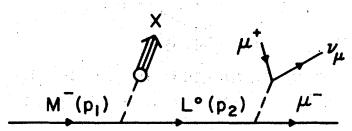

FIG. 2. The cascade decay chain leading to the production of $\mu^-\mu^+$ events in neutrino interactions.

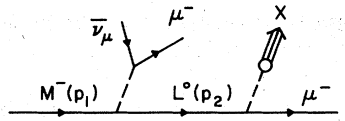

FIG. 3. The cascade decay chain leading to the production of $\mu^-\mu^-$ events in neutrino interactions.

The plan of the paper is as follows: In Sec. II we discuss the production of the M^- in neutrino beams and the production of the M^+ in antineutrino beams. The structure functions of the quark-parton model are used at the production vertex. We discuss transitions from both light-mass quarks to light-mass quarks as well as light-mass quarks to heavy quarks. Then we proceed to discuss the decay modes of the M^- particle and the L^0 particle in Sec. III; estimates are given for decay branching ratios into leptonic and hadronic channels. Sec. IV gives results for the decay chain involving $\mu^-\mu^+$ final states. Then Sec. V has a discussion of $\mu^-\mu^-$ final states. Finally we give the trimuon-event distributions in Sec. VI. In Sec. VII we summarize our results and give our conclusions.

II. M^- PRODUCTION

We begin our discussion of the lepton-cascade processes with the production reaction (for momentum assignments see Fig. 1)

$$\nu_\mu(\bar{\nu}_\mu) + N \to M^\mp + X, \qquad (2.1)$$

occuring off an isoscalar target. The differential cross section is conveniently expressed in terms of the time-reversal-invariant structure functions $W_i = W_i(q^2, \nu)$ according to

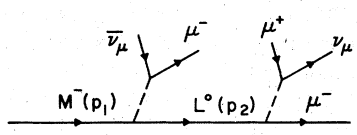

FIG. 4. The cascade decay chain leading to the production of $\mu^-\mu^-\mu^+$ events in neutrino interactions.

$$\frac{d^2\sigma^{\nu,\bar{\nu}}}{dq^2 d\nu} = \frac{G^2}{8\pi E^2}\left\{2(q^2+m^2)W_1^{\nu,\bar{\nu}} + [4E(E-\nu)-(q^2+m^2)]W_2^{\nu,\bar{\nu}} \mp \frac{1}{M}[2Eq^2-\nu(q^2+m^2)]W_3^{\nu,\bar{\nu}} + \frac{m^2}{M^2}[(q^2+m^2)W_4^{\nu,\bar{\nu}} - 2MEW_5^{\nu,\bar{\nu}}]\right\}, \tag{2.2}$$

where $q^2=(k-p_1)^2>0$ and $\nu=-p\cdot q/M=E-E_1$ are the modulus of the four-momentum transfer squared and the energy transfer to the hadrons. M is the nucleon mass, and m is the mass of the heavy lepton. Previous studies have shown that the heavy lepton is produced partially polarized.[14] In its rest frame the polarization vector is given by

$$(\vec{P})_{\nu,\bar{\nu}} = \pm m\left\{\left[2W_1 - W_2 \mp \frac{E}{M}W_3 - \frac{m^2}{M^2}W_4 + \frac{1}{M}(E-\nu)W_5\right]\vec{k} + \left[2\frac{E}{M}W_2 \mp \frac{1}{2M^2}(q^2+m^2)W_3 - \frac{1}{2M^2}(q^2+m^2)W_5\right]\vec{p}\right\} \times \left\{(q^2+m^2)W_1 + \left[2E(E-\nu) - \tfrac{1}{2}(q^2+m^2)\right]W_2 \mp \frac{1}{2M}[2Eq^2-\nu(q^2+m^2)]W_3 + \frac{m^2}{2M^2}[(q^2+m^2)W_4 - 2MEW_5]\right\}^{-1}, \tag{2.3}$$

where $\vec{k}$ and $\vec{p}$ are the momenta of the neutrino and incident nucleon in that frame and the superscripts on the structure functions are suppressed. However, as far as the total cross section is concerned we sum over the final polarizations. In the later sections, where we add on decays into specific channels, polarization effects are taken into account.

One can introduce the usual scaling variables $x=q^2/2M\nu$ and $y=\nu/E$ at this point. We prefer, however, to entertain the possibility that the $\nu_\mu \to M^-$ current may induce a light-to-heavy quark transition at the hadronic vertex. In other words, the gauge-field coupling the leptonic and hadronic currents may differ from the ordinary $W^\pm$ field of the SU(2)-type models. We assume, of course, that the latter field is responsible for the conventional $\nu_\mu \to \mu^-$ transition.

We thus write an effective scaling variable[15]:

$$\xi_j = (q^2+m_j^2)/2M\nu = x + m_j^2/(2MEy), \tag{2.4}$$

which conveniently summarizes much of the nonscaling behavior arising from quark mass corrections to the Bjorken scaling variable. The effective mass of the heavy quark is m_j ($m_j \cong 0$ for light u, d, or s quarks). In terms of this ξ variable, the structure functions are assumed to scale in the Bjorken limit ($E\to\infty$, $q^2\to\infty$, $\nu\to\infty$, q^2/ν fixed) according to

$$\lim MW_1 = F_1(\xi), \quad \lim \nu W_k = F_k(\xi), \quad k=2,3,4,5. \tag{2.5a}$$

The positivity conditions on the W's can be translated into certain restrictions on the F's in the scaling region[16] and one can show that the Callan-Gross[17] relation taken together with the Gross–Llewellyn Smith[18] relation

$$-\xi_j F_3^{(i\to j)}(\xi_j) = B_{ij}F_2^{(i\to j)}(\xi_j) \tag{2.5b}$$

(where $B_{ij}=+1$ for negative-helicity quarks and $B_{ij}=-1$ for positive-helicity quarks) impose restrictions on F_4 and F_5 such that[19]

$$F_4 = 0, \tag{2.5c}$$

$$\xi_j F_5^{(i\to j)}(\xi_j) = F_2^{(i\to j)}(\xi_j). \tag{2.5d}$$

Note that the initial quark is always regarded as a light-mass quark. Relations (2.5a)–(2.5d) are adopted for the structure functions during the rest of our analysis. The F_2 structure function can be approximately expressed in terms of valence and sea parton distribution functions as follows:

$$F_2(\xi) = \xi[u_V(\xi) + d_V(\xi) + 2\eta(\xi)], \tag{2.6}$$

for both light-to-light and light-to-heavy quark transitions. We find that our results for the multimuon decay distributions are insensitive to specific forms of the parton distribution functions. We used both the Pakvasa-Parashar-Tuan[20] parametrization as well as an older form suggested by Llewellyn Smith.[21]

To calculate the $\nu_\mu \to M^-$ inclusive production cross section, we integrate Eq. (2.1) over the q^2-ν plane bounded by the curves

$$2M\nu - q^2 + M^2 = M_B^2 \tag{2.7a}$$

and

$$\nu = E - \frac{q^2+m^2}{4E} - \frac{m^2 E}{q^2+m^2}. \tag{2.7b}$$

The threshold mass, M_B, represents the mass of the lightest baryon carrying the flavor quantum of the heavy quark which has the effective quark mass m_j in Eq. (2.4). In models where the $\nu_\mu \to M^-$ transition couples only light quarks, $M_B = M$; in light-to-heavy transitions $M_B = 5$ GeV/c^2.

The cross-section curves for various choices[22] of the parameters are shown in Fig. 5, along with the cross section for the $\nu_\mu \to \mu^-$ inclusive process $\nu_\mu + N \to \mu^- + X$, which rises linearly with the beam energy. All the curves for M^- production assume its mass to be 8 GeV/c^2 and the coupling strength to be given by G_F. Curve (a) refers to a full-strength $V-A$ interaction which couples d to u quarks through the conventional W^+ field. Curves (b) and (c) refer to $V-A$, $V+A$ coupling of d to c quarks with masses $m_c = 1.5$ GeV/c^2 and $M_c = 2.25$ GeV/c^2, respectively. Note that the threshold for the reaction has changed. If we now allow transitions from d to t quarks, then we choose effective masses $m_t = 4$ GeV/c^2 and $M_t = 5$ GeV/c^2 which shifts the threshold for the reaction up to approximately 90 GeV. Curves (d) and (e) show the total cross sections in this case, assuming $V-A$ and $V+A$ charged-current coupling between the d and t quarks, respectively. The suppression of curves (b), (c), (d), and (e) with respect to (a) is due to a combination of effects such as higher threshold energies, helicity differences, and slow rescaling arising from the effective quark masses.

The trimuon events[7] detected by the FHPRW group were obtained during a run with the quadrupole-triplet-target train. The predicted event rate for M^- production can be found by folding the cross-section curves with the flux spectrum pertinent to that run. In Fig. 6 we plot total cross section times flux versus the beam energy for the curves drawn in Fig. 5, keeping the same labeling. It is clear from Fig. 6 that the event rate for the heavy-lepton production process peaks at around 175 GeV and is nonnegligible at 300 GeV. (For a dichromatic beam such as used by the Caltech-Fermilab collaboration the long tail will not be present in the event rate.) With a low-energy cut on the neutrino energy of $E \geq 100$ GeV, the ratios for the flux-averaged heavy-lepton production cross sections to the flux-averaged $\nu_\mu \to \mu^-$ reaction cross section are found to be 14%, 12%, 5%, 6% and 2% for curves (a)–(e), respectively. These numbers have to be multiplied by branching ratios for M^- and L^0 decays before event rates for $\mu^-\mu^+$, $\mu^-\mu^-$, and $\mu^-\mu^-\mu^+$ events can be given.

We now give results for the antineutrino production of the M^+, based on a mass of 8 GeV/c^2 and coupling constant G_F. In Fig. 7 we show the cross section for μ^+ production via light quarks and M^+

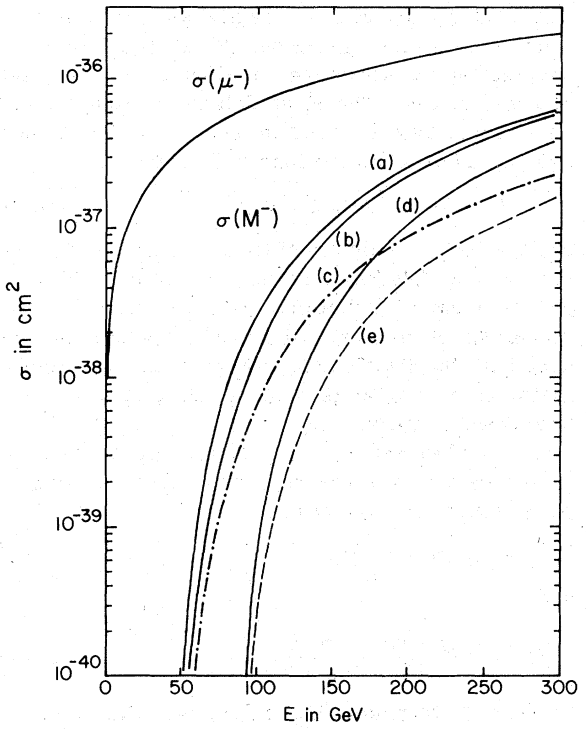

FIG. 5. Total cross sections for the production of the μ^- and the M^- by neutrinos. Curves (a), (b), (c), (d), and (e) refer to M^- production together with light quarks ($V-A$ coupling), charmed quarks, ($V-A$ coupling), ($V+A$ coupling), and heavy quarks ($V-A$ coupling), ($V+A$ coupling), respectively.

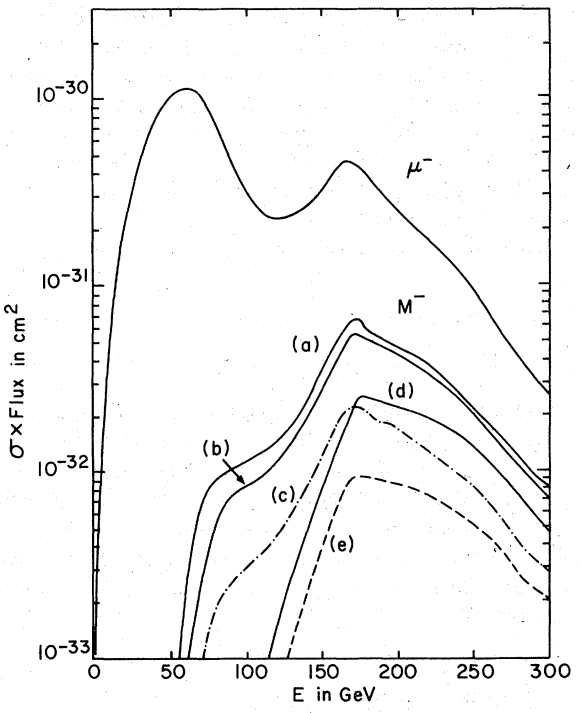

FIG. 6. Total cross section times flux curves for μ^- and M^- production by neutrinos. The curves (a), (b), (c), (d), and (e) refer to M^- production together with light quarks ($V-A$ coupling), charmed quarks ($V-A$ coupling), ($V+A$ coupling) and heavy quarks ($V-A$ coupling), ($V+A$ coupling), respectively.

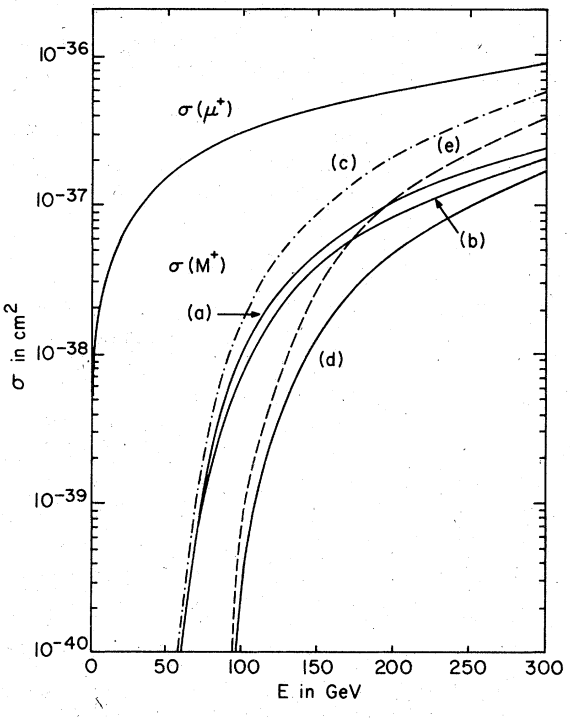

FIG. 7. Total cross sections for the production of μ^+ and M^+ by antineutrinos. The notation is the same as in Fig. 5.

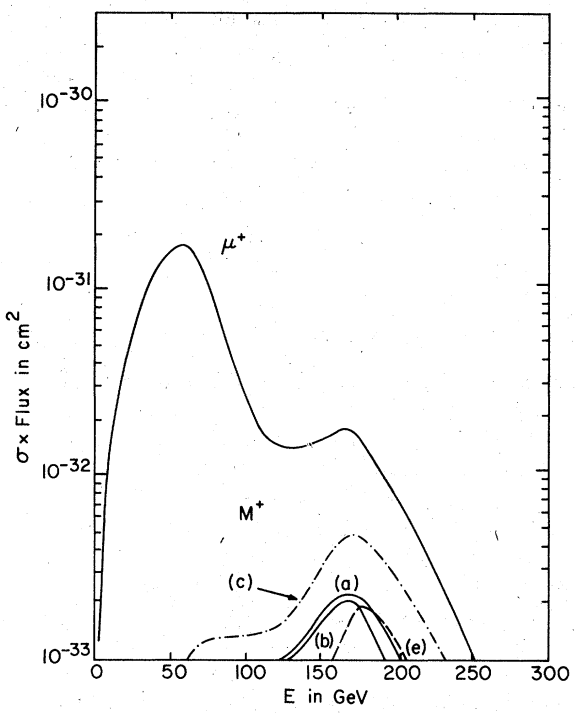

FIG. 8. Total cross section times flux curves for μ^+ and M^+ production by antineutrinos. The notation is the same as in Fig. 6.

production in both light-to-light and light-to-heavy quark transitions. Curve (a) shows M^+ production from light quarks with a $V-A$ coupling to the W^-. Curves (b), (c), (d), and (e) show analogous cross sections for charmed quarks, and heavy quarks with $V-A$ and $V+A$ couplings, respectively, using the same masses as above. Finally, we show the event rate curves for the antineutrino spectrum in Fig. 8. The fact that the antineutrino spectrum falls more sharply than the neutrino spectrum means that total event rates for $\bar{\nu}_\mu$ induced events are much smaller than those for ν_μ induced events, even though the percentage ratios for beam energies larger than 100 GeV are comparable. The corresponding numbers for the ratios of the flux-averaged cross sections are 11%, 9%, 22%, 4%, and 8% for (a)–(e), respectively. The curve (d) is so small that it cannot be drawn on the figure.

If we now compare the ratios for the antineutrino production of the M^+ to the neutrino production of the M^- then we see that it will be much harder to see any trimuon events from M^+ decay in the quadrupole-triplet run. The ratio of regular μ^+ to μ^- event rates is expected to be 4% while the corresponding ratio of M^+ to M^- event rates for $V-A$ and light-to-light quark transitions is 3%, both integrated over beam energies larger than 100 GeV. It is interesting to note that the event rates do change significantly if we insist that the production of the M^- and M^+ is only allowed in light-to-heavy quark transitions. The event-rate ratios for cases (b), (c), (d), and (e) are 3%, 17%, 3%, and 14%, respectively.

III. M^- AND L^0 HEAVY-LEPTON DECAY MODES

Once produced, the M^- heavy lepton has many possible decay modes. In this paper, we shall restrict our attention to charged-current decay modes only since the structure of the neutral current (if present at all) is considerably less certain. The M^- can then decay into the following channels:

$$M^- \to \nu_\mu + \mu^- + \bar{\nu}_\mu , \tag{3.1a}$$

$$M^- \to \nu_\mu + e^- + \bar{\nu}_e , \tag{3.1b}$$

$$M^- \to \nu_\mu + \tau^- + \bar{\nu}_\tau , \tag{3.1c}$$

$$M^- \to \nu_\mu + \text{hadrons} , \tag{3.1d}$$

where τ^- is the heavy lepton of mass ~1.9 GeV/c^2 observed at SPEAR and DORIS and ν_τ is its neutrino. These τ leptons may belong to a new sequential set distinct from the electron or muon type, or they may be identified with a heavy electron and the electron-type neutrino ν_e.[23]

In order to produce trimuon and same-sign di-

muon events through leptonic channels, it is necessary to postulate the existence of at least one neutral lepton L^0, with a smaller mass than the M^-. If only charged-current decay channels are present, the L^0 is in fact a heavy-muon neutrino. Additional M^- decay channels open are

$$M^- \to L^0 + \mu^- + \bar{\nu}_\mu , \tag{3.1e}$$

$$M^- \to L^0 + e^- + \bar{\nu}_e , \tag{3.1f}$$

$$M^- \to L^0 + \tau^- + \bar{\nu}_\tau , \tag{3.1g}$$

$$M^- \to L^0 + \text{hadrons} . \tag{3.1h}$$

Since less phase space is available for the second set of decay modes, the branching ratios for (3.1e)–(3.1h) are somewhat smaller than their (3.1a)–(3.1d) counterparts. Reasonable estimates lead to branching ratios of 5%–10% and 20%–30%, respectively, for the two decay modes (3.1e) and (3.1h) of interest to us in this paper. While one can calculate these decay branching ratios precisely in specific gauge models, we feel that this approach is rather premature so we use the members quoted above.[24]

Once produced, the L^0 heavy lepton can decay into the following (charged-current) decay channels:

$$L^0 \to \mu^- + \nu_\mu + \mu^+ , \tag{3.2a}$$

$$L^0 \to \mu^- + \nu_e + e^+ , \tag{3.2b}$$

$$L^0 \to \mu^- + \nu_\tau + \tau^+ \quad (\text{if } m_{L^0} > m_\tau + m_\mu) \tag{3.2c}$$

$$L^0 \to \mu^- + \text{hadrons} . \tag{3.2d}$$

Neglecting neutral-current channels, reasonable estimates lead to branching ratios of 10%–15% and 50%–60%, respectively, for the (3.2a) and (3.2d) decay modes. Of course, in different modes a given decay mode may be enhanced or suppressed by a particular current–gauge-field coupling.

Trimuon events then arise through the (3.1e) and (3.2a) decay chain. Our estimate of the product branching ratio is then of the order of

$$B(M^- \to L^0 \mu^- \bar{\nu}_\mu)\, B(L^0 \to \mu^- \nu_\mu \mu^+) \approx (0.5\text{–}1.5)\% . \tag{3.3}$$

The estimated production cross section times branching ratios is then of the order

$$\frac{\sigma(\nu_\mu \to \mu^- \mu^- \mu^+)}{\sigma(\nu_\mu \to \mu^-)} \sim (1\text{–}20) \times 10^{-4} , \tag{3.4}$$

for the energy cut $E \geq 100$ GeV and the various quark transitions considered above. This number is to be compared with the uncorrected experimental number, 5×10^{-4}, based on six trimuon events from the FHPRW collaboration. Estimates of the detection efficiencies have not been made at the time of this writing.

The same-sign dimuon events ($\mu^-\mu^-$) arise from the decay chain (3.1e) followed by (3.2d). In the counter experiments, which are insensitive to electrons, the decay chain (3.1e) followed by (3.2b) will also serve as a source of same-sign dimuon events. The product branching ratio can then be estimated to be

$$B(M^- \to L^0 \mu^- \bar{\nu}_\mu) B(L^0 \to \mu^- X) \simeq (3\text{–}7.5)\% . \tag{3.5}$$

Comparison of the branching ratios of L^0 decay suggests that same-sign dimuons should be

$$\frac{\sigma(\nu \to \mu^- \mu^-)}{\sigma(\nu \to \mu^- \mu^- \mu^+)} \sim 4\text{–}8 \tag{3.6}$$

times more abundant than the trimuon events observed. This estimate is compatible with the experimental finding.[25] Note, however, that experimental cuts can be very important in making any comparison between multimuon event rates.

Regarding the opposite-sign dimuons ($\mu^-\mu^+$), we note that they can originate from the (3.1h) and (3.2a) decay chain, as well as the (3.1f) and (3.2a) decay chain, when the electron is not detected by the counter experiments. However, if a neutral-current ν_μ-L^0 coupling exists, opposite-sign dimuons can be produced directly from the L^0 production and decay. The muon distributions for this process have been studied at some length, independently, by Chang, Derman, and Ng and by Albright.[6] Ignoring this possible neutral-current coupling, the ratio of opposite-sign to same-sign dimuons is estimated to be in the range

$$\frac{\sigma(\nu \to \mu^- \mu^+)}{\sigma(\nu \to \mu^- \mu^-)} \sim 0.3\text{–}2 . \tag{3.7}$$

This number is in poor agreement with the experiments[5] which indiacte a ratio ~10. Indeed, most of the opposite-sign dimuon events have been interpreted as arising from single-charmed-particle production by charged-current coupling $\nu_\mu \to \mu^-$ followed by semileptonic decay into the muon mode.[26]

IV. OPPOSITE-SIGN DIMUON PRODUCTION

We now turn our attention to a detailed discussion of the dimuon and trimuon distributions which can be compared with experiment. In order to present a coherent picture, we shall consider primarily $V-A$ couplings and light-to-light quark transitions and simply comment on the changes observed with somewhat different couplings. We have chosen $m_M = 8$ GeV/c^2 and $m_L = 4$ GeV/c^2 to illustrate most of our results.

We first take up the subject of opposite-sign dimuon ($\mu^-\mu^+$) production. Though this process, occurring mainly through the production and de-

cay chain shown in Fig. 2, must compete with the large background due to semileptonic decay of singly produced charmed particles, it is somewhat simpler to analyze than the same-sign dimuon production since the muons are distinguishable. We shall present flux-averaged results based on the FHPRW quadrupole-triplet-target spectrum and impose the following experimental cuts on all the muon energies and angles:

$$E_\mu > 4 \text{ GeV}, \tag{4.1a}$$

$$\theta_\mu < 400 \text{ mrad}. \tag{4.1b}$$

These experimental cuts applicable to the FHPRW setup approximate the average muon energy and opening angle necessary to ensure detection and identification of the muons.

The actual calculation of the polarized M^- particle decay into the channel L^0+X is relatively simple.[1] We introduce the structure function $W_1(s)$ related to the e^+e^- total cross-section ratio R by

$$W_1(s) = \frac{1}{4\pi} R(s) = \frac{1}{4\pi} \frac{\sigma(e^+e^- \to \text{hadrons})}{\sigma(e^+e^- \to \mu^+\mu^-)}. \tag{4.2}$$

The experimental value for R is larger than unity in the energy range required.[27] As an approximation to $R(s)$ in the range $1 \text{ GeV}^2 < s < (m_M - m_L)^2$, we use the simple form[28]

$$R(s) = \tfrac{1}{3}(1+2\sqrt{s}), \quad s \geq 1 \text{ GeV}^2. \tag{4.3}$$

Hence the decay of the M^- is given by

$$\frac{d\Gamma(M^- \to L^0+X)}{d^4p_2} = \frac{G^2}{(2\pi)^3}\frac{1}{m_M}[(m_M^2 - m_L^2)^2 + (m_M^2 + m_L^2)s - 2s^2 + 2m_M(\vec{s}\cdot\vec{p}_L)(2s - m_M^2 + m_L^2)]W_1(s), \tag{4.4}$$

where $\vec{s}$ is the spin vector of M^-, and we do not write the δ and θ functions explicitly. The distributions can now be calculated by folding Eq. (4.4) with Eq. (2.3). Note that the L^0 polarization is not included because we expect its effects to be very small.[29] We then add the matrix element for the decay of the unpolarized L^0 into the channel $L^0 \to \mu^- + \mu^+ + \nu_\mu$. The distributions which follow were generated by a Monte Carlo routine using approximately one thousand points. With this relatively small number there is still some scatter on the distributions so our curves have errors of roughly 5–10%. This accuracy is quite sufficient for our present purposes. Small differences caused by varying parameters will be extremely difficult to verify experimentally. We will comment on these changes at the end of this section.

In Fig. 9 the energy spectra are given for the muons, $E^- \equiv E_{\mu^-}$, $E^+ \equiv E_{\mu^+}$, the missing neutrino, the hadronic energy, the visible, and the total energy. All three leptons (μ^-, μ^+, and ν_μ) show quite similar spectra which are peaked around 15 GeV with tails extending up to over 100 GeV. The hadronic energy, on the other hand, shows a broad spectrum which extends from 0 to 250 GeV and peaks around 75 GeV. The visible energy, $E_{\text{vis}} = E^- + E^+ + E_{\text{had}}$ peaks near 150 GeV while the total energy, $E_{\text{tot}} = E_{\text{vis}} + E_{\nu_\mu}$, peaks around 175 GeV for the quadrupole-triplet spectrum. This is consistent with our previous calculation of the event rate for M^- production (see Fig. 6). We also show the distributions in the ratios of the muon energies to the visible energy $z^\pm = E^\pm/E_{\text{vis}}$ and $z'_+ = E^+/(E_{\text{vis}} - E^-)$ in Fig. 10. These distributions peak for low values of the variables.

The correlation between μ^- and μ^+ momenta are shown in the scatter plot of Fig. 11, where the cuts of (4.1) have not been applied. It is clear that most of the events have small energies

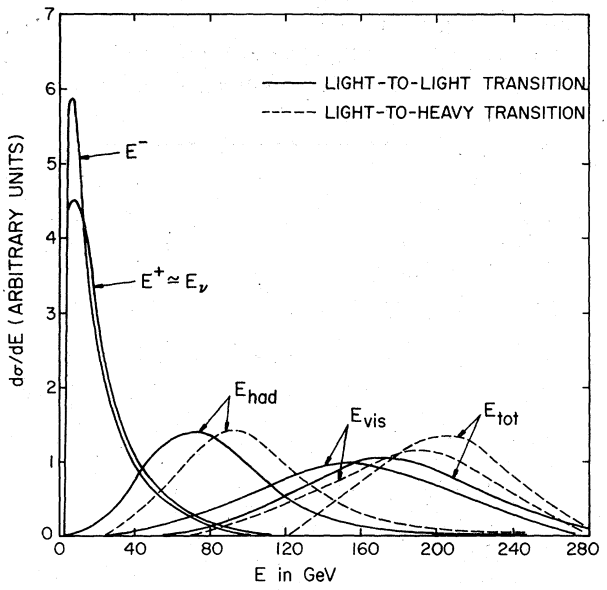

FIG. 9. Energy distributions for the μ^-, μ^+, the missing energy E_ν the hadronic energy E_{had}, the visible energy E_{vis}, and the total energy E_{tot}, all flux-averaged with the quadrupole-triplet spectrum. The solid curves refer to light-to-light quark transitions while the dashed curves refer to light-to-heavy quark transitions.

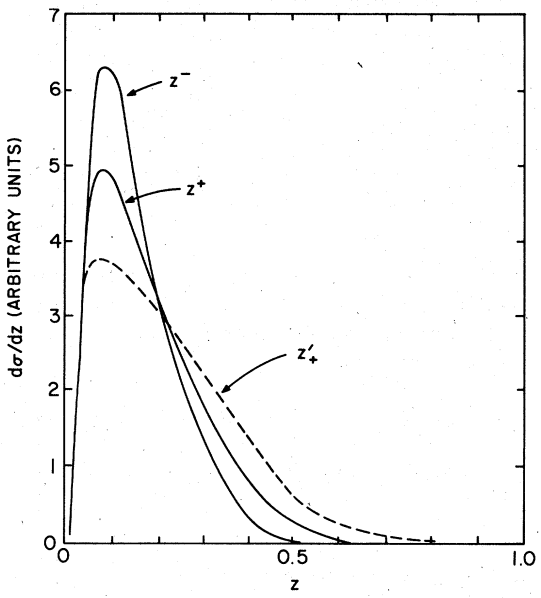

FIG. 10. The distributions in $z^{\pm}=E^{\pm}/E_{\rm vis}$ and $z'_{+}=E^{+}/(E_{\rm vis}-E^{-})$.

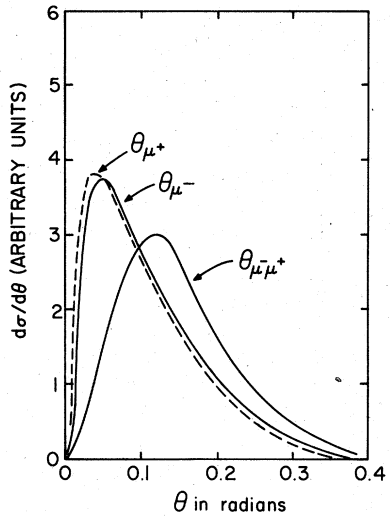

FIG. 12. Polar angles of the μ^- and μ^+ relative to the neutrino beam direction and the $\mu^-\mu^+$ opening angle.

$(p_{\mu^-}, p_{\mu^+} \lesssim 30$ GeV/$c)$, but a sizable number of events are found where the two muons carry off a substantial amount of energy. These so-called "symmetric" dimuons stand out from the background due to single-charmed-particle production and decay.[25] The latter process yields muons which are limited to the region $E^+ \lesssim 40$ GeV, while E^- is generally $\lesssim 150$ GeV.

The muon angles relative to the neutrino beam direction are shown in Fig. 12 along with the opening angle $\theta_{\mu^-\mu^+}$. The μ^+ angle is peaked slightly lower than the μ^- angle, though for both $\theta_{\rm max} \sim 50$ mrad. The opening angle peaks at a slightly larger value and extends out to 400 mrad. The θ_{μ^-}-θ_{μ^+} scatter plot in Fig. 13 shows a rather symmetrical distribution.

In Fig. 14 we depict the theoretical prediction for the invariant masses of the dimuons, $M_{\mu^-\mu^+}$, as well as that of the hadrons $M_{\rm had}$. Since we have chosen a mass of 4 GeV/c^2 for the L^0, the μ^--μ^+ invariant mass is constrained to lie below this value. It is slightly skewed to mass values greater than 2 GeV/c^2 due to the assumed $V-A$ form of the interaction. For light-to-light quark transi-

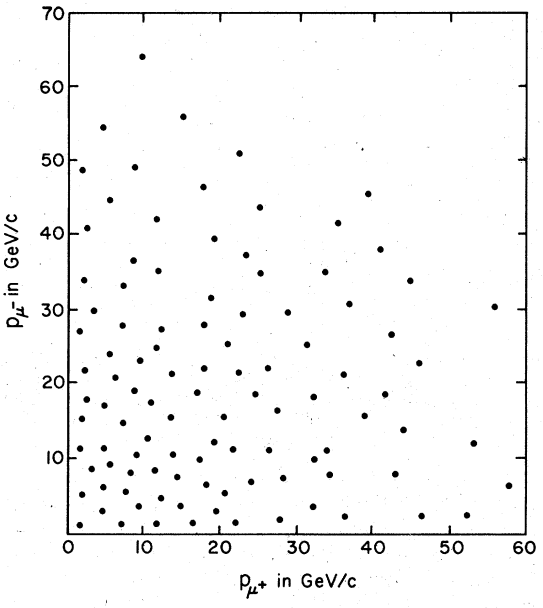

FIG. 11. Scatter plot of p_{μ^-} versus p_{μ^+}.

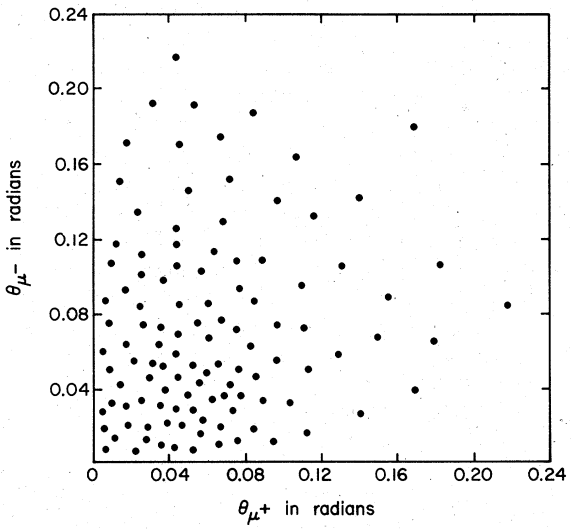

FIG. 13. Scatter plot of θ_{μ^-} versus θ_{μ^+}.

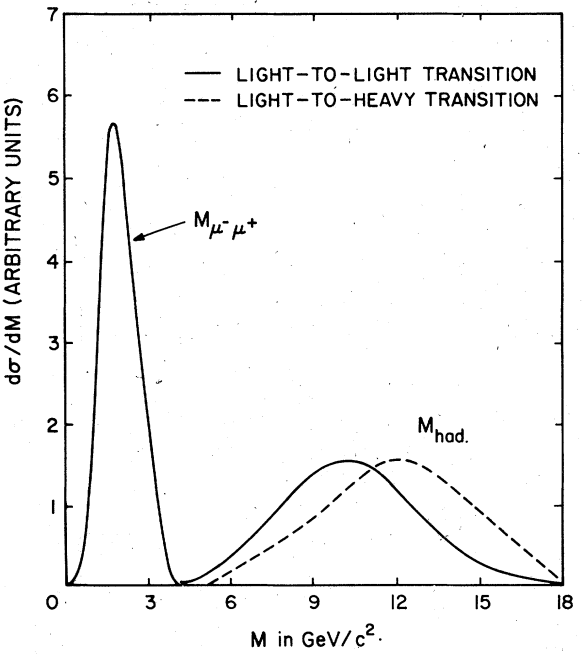

FIG. 14. Invariant masses of the dimuons and hadrons. The solid curves refer to light-to-light quark transitions while the dashed curve refers to light-to-heavy quark transitions.

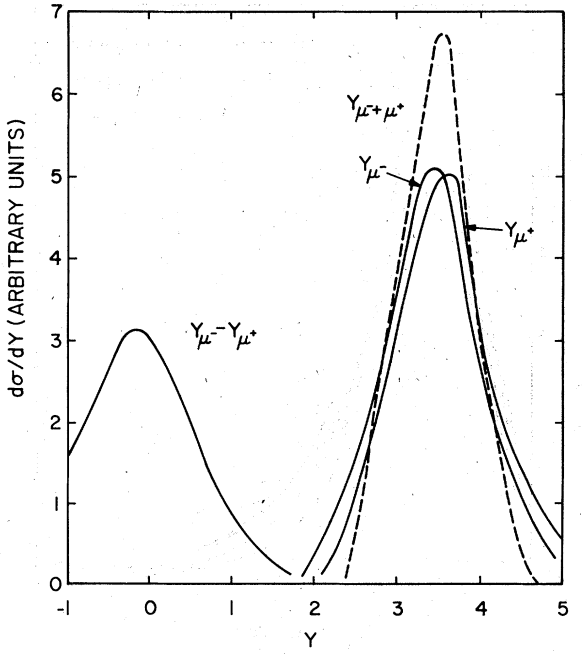

FIG. 15. Rapidity plots for the μ^-, μ^+, $(\mu^-+\mu^+)$, and the rapidity gap between μ^- and μ^+.

tions, the invariant-hadronic-mass spectrum is broad, extending from 4 GeV/c^2 to 19 GeV/c^2 and peaking near 11 GeV/c^2. This broad range results from the fact that hadrons are produced directly in the ν_μ-M^- process as well as in the decay channel $M^- \to L^0$ +hadrons. The corresponding light-to-heavy quark transition yields a broader M_{had} distribution which peaks at even larger values.

The leading-particle effects of the dimuons can be seen clearly from the rapidity plot in Fig. 15, where Y_{μ^-}, Y_{μ^+}, $Y_{\mu^-}-Y_{\mu^+}$, and $Y_{(\mu^-+\mu^+)}$ are given. We have defined

$$Y = 0.5 \ln\left(\frac{E+p_z}{E-p_z}\right), \tag{4.5}$$

where p_z is the component of the momentum along the neutrino beam direction. The rapidity peaks are narrow and maxima occur for $Y \sim 3.5$. The rapidity gap, $Y_{\mu^-} - Y_{\mu^+}$, is peaked just below zero.

We now discuss the projections of the momenta onto different planes. There are several possibilities here so our aim is to try to find distributions which maximize the difference between theoretical models. Hence we deliberately make projections along different sets of axes. To make the discussion systematic, we introduce three different (x, y) planes. The first one is the (x, y) plane orthogonal to the neutrino beam direction, which we naturally take to be the z axis. The second plane is defined by assuming that there is a regular ν_μ-μ^- transition at a leptonic vertex where a W boson is emitted. As an approximation to this picture one calculates the total visible energy in the event and assigns this value to the incoming neutrino. One then forms the W-boson three-vector from the difference between the visible neutrino three-vector and the measured μ^- three-vector. A z' axis is then defined along the W direction and a (x', y') plane is set up orthogonal to the z' axis.

In our model it is natural to choose another W-boson direction, i.e., the one emitted at the ν_μ-M^- transition vertex. To approach this as close as possible we again assign to the neutrino the total visible energy but we calculate the approximate W-boson direction from the difference between the visible neutrino three vector and the sum of the three vectors of the visible muons. This W-boson direction is taken to be the z'' axis and again we set up an (x'', y'') plane orthogonal to it. We can project the muon three vectors onto each of these planes and form (p_x, p_y, p_z), (p'_x, p'_y, p'_z), and (p''_x, p''_y, p''_z). Also, the transverse momenta $p_\perp$, $p'_\perp$, $p''_\perp$, and the angular correlations between these vectors can be studied. These angles we call ϕ_{12}, ϕ'_{12}, ϕ''_{12}, etc., where the subscripts identify the muons.

The muon transverse momenta are shown in Fig. 16. Relative to the neutrino beam direction,

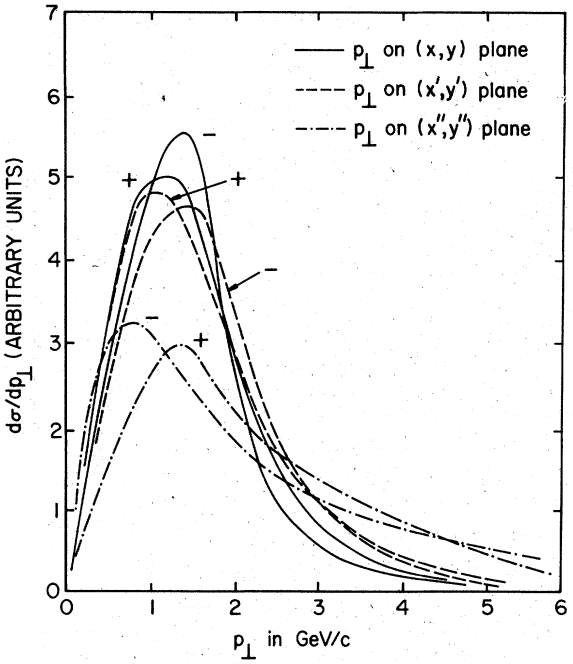

FIG. 16. The spectra in the transverse muon momenta (+ and − refer to the μ^+ and μ^-, respectively).

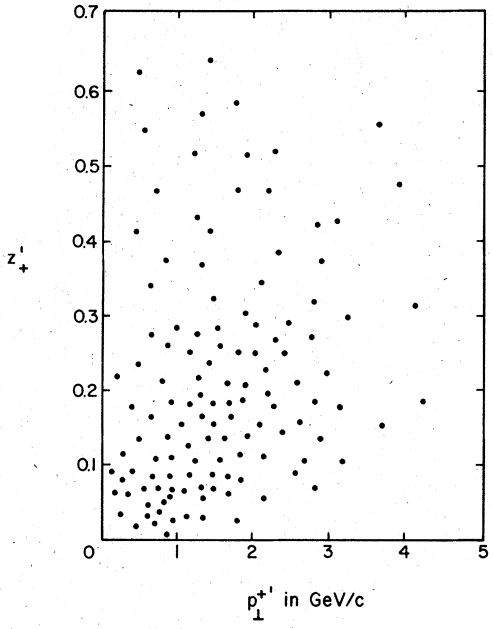

FIG. 17. Scatter plot of $p'_\perp$ versus z'_+ for the positive muon.

the transverse momenta of the μ^- and the μ^+ peak around 1.5 GeV/c and extend out to ~6 GeV/c. The distributions for the $p_\perp$ projections along the other axes reflect the fact that the approximate W-boson axes are skewed with respect to the neutrino direction. Most of the distributions have long tails extending out to $p_\perp$ values as large as 7 GeV/c. With respect to the (x', y') plane, which is most relevant for a charmed-particle-decay interpretation of the $\mu^-\mu^+$ events, the maxima in the $p'_\perp$ distributions are approximately 1.5 GeV/c and the average $p'_\perp$ values are even larger. This behavior should be compared with that expected from charmed-particle production and decay, where the $p_\perp$ values are considerably smaller. We also show a two-dimensional scatter plot of $p'_\perp$ versus z'_+ for the positive muon in Fig. 17. Note that there are many events with relatively large $p_\perp$ and large values of z'.

The azimuthal opening angles of the dimuon pair ϕ_{-+}, ϕ'_{-+}, ϕ''_{-+} are given in Fig. 18. These plots show that the relatively flat ϕ_{-+} distribution becomes more peaked towards the zero opening angle as we move to the other axes. The relatively flat behavior of ϕ_{-+} results from the fact that the dimuons (together with the missing neutrino) are emitted at uncorrelated azimuthal angles relative to the L^0 direction. When we project on the (x', y') and (x'', y'') planes we are in the situation where the W boson is emitted at a large angle with respect to the neutrino beam so both the muon (and neutrino) directions are on the same side of the z' or z'' axes. The situation is reversed when the muons are considered to be the decay products of hadrons (charmed or not). Then the distribution in ϕ'_{-+} is expected to be flatter than ϕ_{-+} and ϕ''_{-+}. A scatter plot giving the correlation between ϕ_{-+}

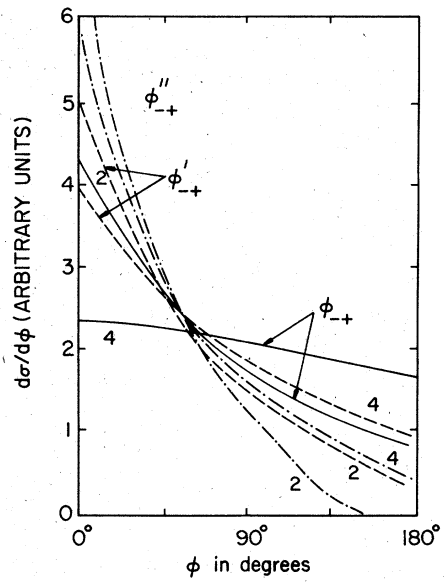

FIG. 18. The distributions in the aximuthal opening angles ϕ_{-+}, ϕ'_{-+}, and ϕ''_{-+}. The curves marked 2 and 4 refer to $m_L = 2$ GeV/c^2 and $m_L = 4$ GeV/c^2, respectively.

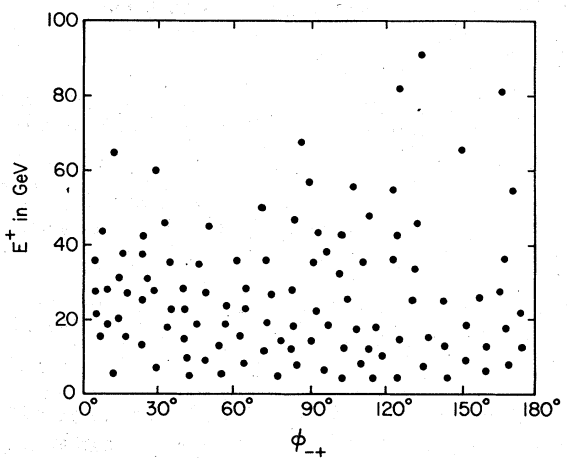

FIG. 19. Scatter plot of ϕ_{-+} versus E^+.

and E^+ is shown in Fig. 19. Note that some events extend out to values of $E^+ \simeq 60$ GeV for the full range of azimuthal angles. We do not give the corresponding distributions for ϕ'_{-+} versus E^+ and ϕ''_{-+} versus E^+. These show more of an accumulation of events for small angles as can be expected from our knowledge of the one-dimensional distributions for ϕ'_{-+} and ϕ''_{-+}.

In Fig. 20 we present the x and y distributions for the production of the M^- particle. We also give the $x_{\rm vis}$ distribution where

$$x_{\rm vis} = \frac{q_{\rm vis}^{\ 2}}{2ME_{\rm had}}, \tag{4.6}$$

with $q^{\ 2}$ defined for the μ^- relative to the visible energy neutrino. This is very peaked toward small x and falls more rapidly than the standard x distribution for the single-μ^- events. We do not find any events with $x_{\rm vis}$ larger than unity. The $y_{\rm vis}$ distribution, also shown in Fig. 20, where $y_{\rm vis}$ is defined by

$$y_{\rm vis} = \frac{E_{\rm had}}{E_{\rm vis}} \tag{4.7}$$

is skewed toward high y values, peaking around $y_{\rm vis} = 0.8$. This behavior is in marked contrast to the flat y distribution measured for the $\nu_\mu + N \to \mu^- + X$ events. The charm process is expected to deviate little from a uniform y distribution so this variable could provide a clear test for the heavy-lepton cascade contribution to the dimuon events.[12]

We close this section by making some comments about the distributions for other quark transitions, different mass assignments, $V+A$ rather than $V-A$ couplings, and $\mu^+\mu^-$ production in antineutrino beams. The effects of these changes have been extensively investigated but it is difficult to add all these results to our figures.

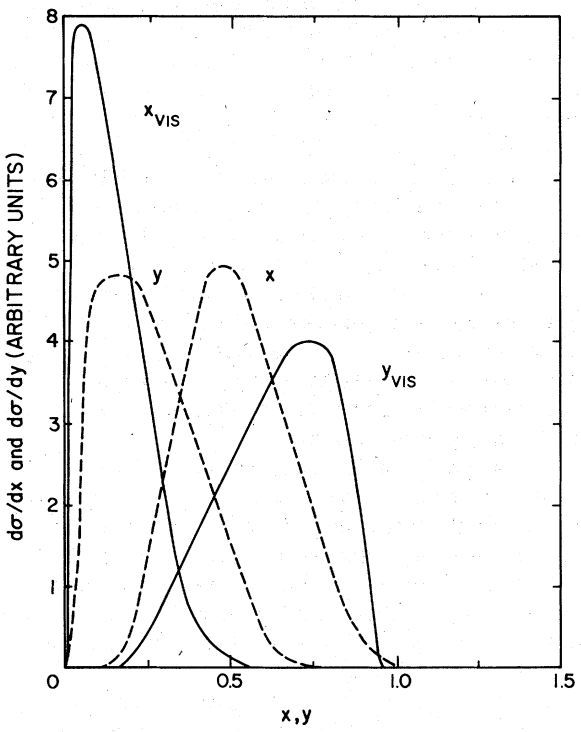

FIG. 20. The distributions in x, y for the production of the M^- and $x_{\rm vis}, y_{\rm vis}$ defined with respect to the μ^-.

In general the effect of taking light-to-heavy quark transitions at the hadronic vertex is to reduce the production cross section and to change the spectra in $E_{\rm had}$, $E_{\rm vis}$, and $E_{\rm tot}$ so that they peak at larger values. In Fig. 9 we showed the results for these distributions as dashed curves. The hadronic energy is obviously pushed to a higher threshold because we insist that $M_B = 5$ GeV/c^2. These changes reflect themselves in the z distributions by making the curves fall off faster than is shown in Fig. 10. This feature stems from the higher $E_{\rm vis}$ as well as the slightly lower energies of the muons. Actually the changes in the muon energy spectra (and the other distributions for the decay muons) are all rather small. In Fig. 14 we show the $M_{\rm had}$ distribution with light-to-heavy quark transitions. The actual position of the threshold depends on the mass assumed for M_B. Our $x_{\rm vis}$ and $y_{\rm vis}$ plots are also changed to make $x_{\rm vis}$ peak at lower x and $y_{\rm vis}$ peak at higher y.

Regarding changes in the M^- and L^0 masses the situation is more complex. The kinematical limits on the decay distributions are set by these masses. Lowering the mass of the M^- increases the overall production rate and reduces the maximum values for the $p_\perp$ distributions for the decay

muons. Lowering the mass of the L^0 changes the spectra rather dramatically because the phase space available for the $M^- \to L^0$ transition is increased while the phase space for the L^0 decay is reduced. Careful analysis of the invariant mass of those $\mu^-\mu^+$ events which are outside the region populated by muons from charmed-particle decay may yield an estimate for the L^0 mass. In general, such mass changes will have to be investigated simultaneously in all the multimuon channels. We note here that the φ distributions are quite sensitive to changes in the L^0 mass. In Fig. 18 we see that lowering the mass of the L^0 increases the φ distributions near zero degrees to reflect the decrease in the p_1 values for the positive and negative muons.

We have arbitrarily chosen $V-A$ couplings for the heavy lepton decays. The differences between $V-A$ and $V+A$ are rather small. From a careful examination of our results we conclude that it will be extremely difficult to see any effects due to changing these relative couplings. The distributions are much more sensitive to the choice of the M^- and L^0 masses.

In this section we have concentrated on $\mu^-\mu^+$ production in a ν_μ beam. Using a $\bar{\nu}_\mu$ beam we can produce $\mu^+\mu^-$ events albeit with a much lower rate. The distributions for the decay muons are now interchanged. Also, the x and y distributions change slightly. The kinematics of the production process $\bar{\nu}_\mu + N \to M^+ + X$ continues to dominate the reaction.[14] For a heavy M^+ particle this means that the regions of small x and large y are the most important regions. The situation is completely different from the usual inclusive μ^+ production where the mass of the muon is negligible. It is well known that the production of a heavy lepton can lead to a high-y anomaly in antineutrino reactions, so these effects were not unexpected.

V. SAME-SIGN DIMUON EVENTS

Analysis of the same-sign dimuon events arising from the decay chain of Fig. 3 is complicated by the identity of the two muons, so that one cannot distinguish which muon came from the M^- decay as opposed to the L^0 decay. This difficulty can be surmounted by separating the muons into $\mu_1^- \equiv \mu_{\text{fast}}^-$ and $\mu_2^- \equiv \mu_{\text{slow}}^-$. We shall do this in all distributions and comment on the main differences between the same-sign and opposite-sign dimuons.

The calculation of the decay chain is made along the same lines as that in Sec. IV. We first compute the decay of a polarized M^- particle into $L^0 + \nu_\mu + \mu^-$ and then add the decay of the unpolarized L^0 into $\mu^- + X$. The amplitude is given, using $M^-(p_1) \to L^0(p_2) + \mu^-(k_1) + \bar{\nu}_\mu(k_2)$, as follows:

$$|\mathfrak{M}(M^- \to L^0 + \mu^- + \bar{\nu}_\mu)|^2 = \frac{96}{\pi^2}\frac{1}{m_M^6}(p_1\cdot k_2\, p_2\cdot k_1 - m_M s_1\cdot k_2\, p_2\cdot k_1)/D, \tag{5.1}$$

where we have divided by a factor D to normalize the decay rate to unity, i.e.,

$$D=(1+\eta)(1-\eta)\left[(1-\eta)^2-\eta-\tfrac{1}{2}(1+\eta)^2+12\eta^2\ln\frac{m_M}{m_L}\right] \tag{5.2}$$

and $\eta = m_L^2/m_M^2$. We have summed over the polarization of the L^0 and used s_1 as the polarization vector of the M^-. Folding Eq. (5.1) with Eq. (2.3) gives the matrix element for the production of the L^0. The final step involves the decay rate of the unpolarized L^0,

$$\frac{d\Gamma}{d^4p}=\frac{G^2}{(2\pi)^3}\frac{1}{m_L}(m_L^2-s)(m_L^2+2s)W_1(s) \tag{5.3}$$

for $L^0 \to \mu^- + X$, if we neglect the mass of the μ^-. For the structure function $W_1(s)$ we use the same form as in Eq. (4.3).

The calculation of the distributions now follows straightforwardly. The energy distribution of the muons, the missing energy, the hadronic energy, visible energy, and total energy are given in Fig. 21. The last three distributions are nearly the

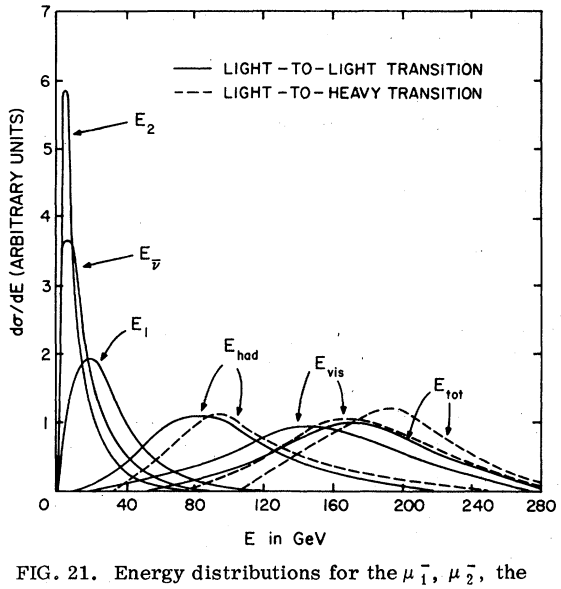

FIG. 21. Energy distributions for the μ_1^-, μ_2^-, the missing energy $E_{\bar{\nu}}$, the hadronic energy E_{had}, the visible energy E_{vis}, and the total energy E_{tot}, all flux-averaged with the quadrupole-triplet spectrum. The solid curves refer to light-to-light quark transitions while the dashed curves refer to light-to-heavy quark transitions.

same as in Fig. 9. The fast-muon energy peaks around 25 GeV and extends out to 150 GeV while the slow-muon energy lies below 75 GeV and peaks around 10 GeV. If we did not order them according to their energy, the two distributions would be more similar. In Fig. 22 we show the distributions in $z_1^- = E_1^-/E_{\rm vis}$, $z_2^- = E_2^-/E_{\rm vis}$, and $z_2^{-\prime} = E_2^-/(E_{\rm vis} - E_1^-)$. The two-dimensional scatter plot of p_1^- versus p_2^- is shown in Fig. 23. The effect of ordering the particles according to their energy is rather obvious. Although the maxima occur for small momenta, there are clearly many events at large p_1.

The fast-muon polar angle relative to the neutrino beam direction, depicted in Fig. 24, is very compressed, peaking below 50 mrad and extending only to 200 mrad. The slow-muon polar angle extends to 400 mrad and peaks at 100 mrad. The relative $\mu^-\mu^-$ opening angle plot is very similar to that for the $\mu^-\mu^+$ opening angle of Fig. 12. The scatter plot of θ_1^- versus θ_2^- in Fig. 25 shows that the fast muon tends to be emitted at a smaller angle than the slow muon.

The invariant-mass plot, Fig. 26, for the dimuon mass $M_{\mu^-\mu^-}$ peaks around 3 GeV/c^2 and extends to ~7 GeV/c^2 in contrast to the $M_{\mu^-\mu^+}$ plot. This occurs since the invariant $\mu^-\mu^-$ mass is constrained only by the mass of the M^- particle which we have taken to be 8 GeV/c^2. The invariant mass of the hadrons appears to peak at a slightly higher value (12 GeV/c^2) compared with that given in Fig. 14.

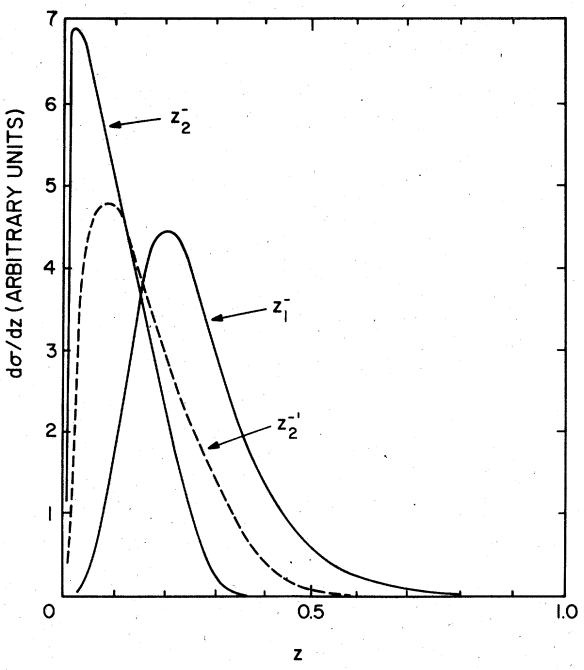

FIG. 22. The distributions in $z_1^- = E_1^-/E_{\rm vis}$, $z_2^- = E_2^-/E_{\rm vis}$, and $z_2^{-\prime} = E_2^-/(E_{\rm vis} - E_1^-)$.

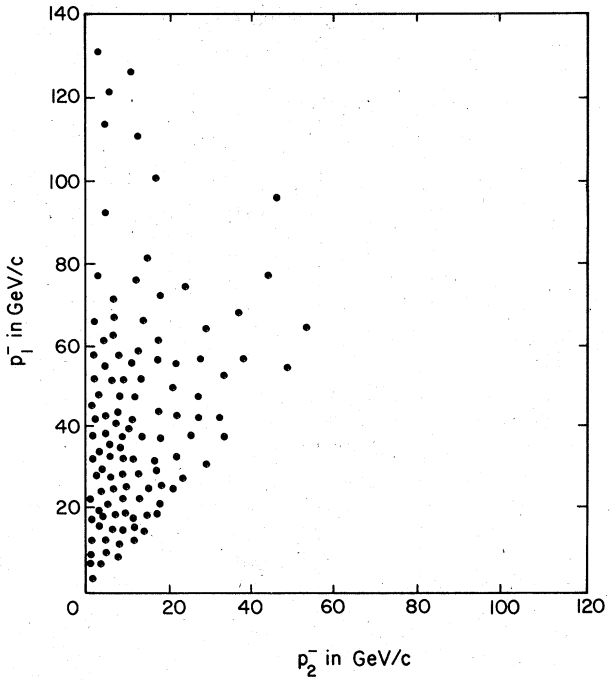

FIG. 23. The scatter plot of p_1^- versus p_2^-.

We also show the invariant mass when the L^0 mass equals 2 GeV/c^2. The change is so small that it will be difficult to use this channel to determine the L^0 mass.

The rapidity plots for the muons are qualitatively similar to those shown in Fig. 15, and are not given. We simply point out that the rapidity for the fast muon peaks at 3.5, while that for the slow muon peaks between 2.5 and 3.0. The peak in the rapidity gap occurs between 0.5 and 1.0.

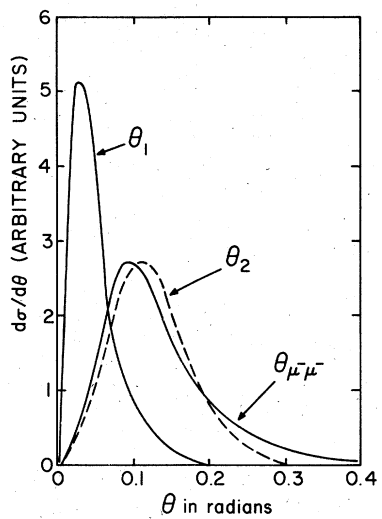

FIG. 24. The polar angles of μ_1^- and μ_2^- relative to the neutrino beam as well as the $\mu_1^-\mu_2^-$ opening angle.

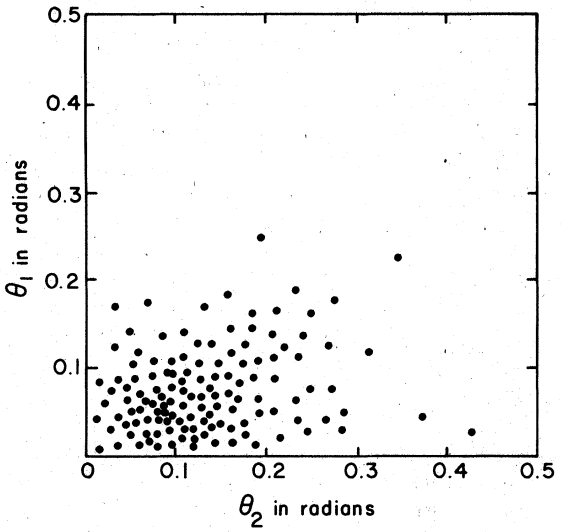

FIG. 25. Scatter plot of $\theta_1 = \theta_{\mu\text{-fast}}$ versus $\theta_2 = \theta_{\mu\text{-slow}}$.

The muon transverse momenta are shown in Fig. 27. The distribution relative to the beam direction is broad for the fast muon and narrow for the slow muon, as expected, with the former peaking near 1.2 GeV/c while the latter peaks at 1.8 GeV/c. Relative to the W-boson axis, which is defined with respect to the fast μ^-, the transverse momentum distributions peak at the same values. The peaks move to slightly larger $p_\perp$ values when we define the W-boson axis with respect to the sum of the two muon momenta. All the distributions

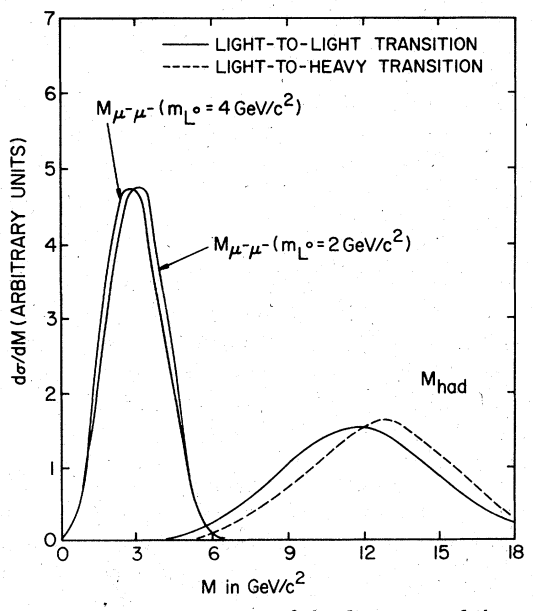

FIG. 26. Invariant masses of the dimuons and the hadrons. The solid curves refer to light-to-light quark transitions while the dashed curve refers to light-to-heavy quark transitions.

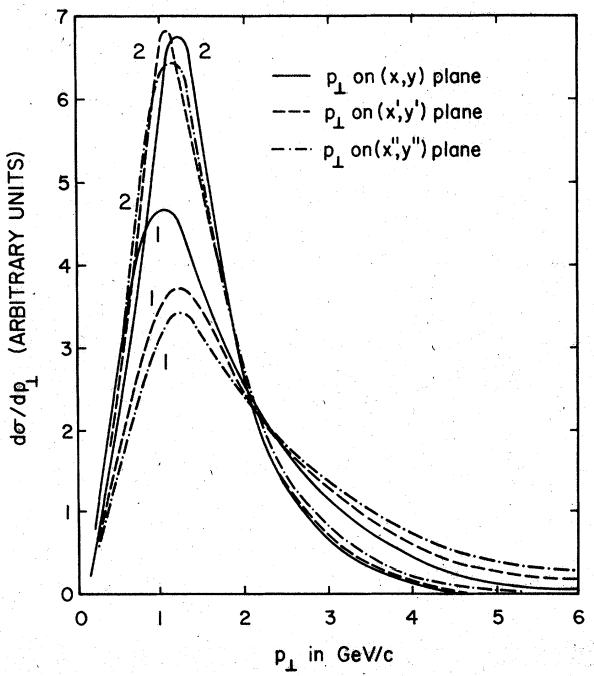

FIG. 27. The spectra in the transverse muon momenta (1 and 2 refer to μ_1 and μ_2, respectively).

have long tails extending above 4 GeV/c. In Fig. 28 we show the two-dimensional scatter plot of $p'_\perp$ versus z'_2 for the slow muon. This distribution can be used to distinguish between the leptonic-cascade hypothesis and a hadronic- (new or

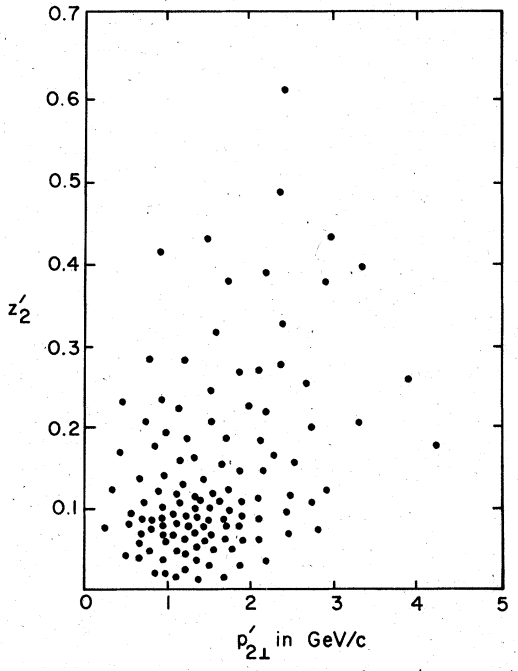

FIG. 28. Scatter plot of $p'_\perp$ versus $z'_2 = E_2/(E_{vis} - E_1)$ for the slow muon.

charmed quarks) cascade hypothesis.

We now turn to the distributions in the angle between the muon vectors projected onto the different planes. The expected spectra for ϕ_{--}, ϕ'_{--}, and ϕ''_{--} are shown in Fig. 29, where we order the muon energies in each event. Obviously the angle in the (x,y) plane is relatively flat and becomes more peaked near small angles as we move to the (x',y') and (x'',y'') planes. For completeness we show a two-dimensional scatter plot of ϕ_{--} versus E_2 in Fig. 30. The slow-muon momentum extends out to approximately 40 GeV independent of ϕ_{--}. The plots of ϕ'_{--} and ϕ''_{--} versus E_2 are similar but have more events near small angles reflecting the changes in the single differential distributions.

In Fig. 31 we show the distributions in x and y for the production of the M^-, and the $x_{\rm vis}$ and $y_{\rm vis}$ distributions computed with respect to the fast μ^-. We again note that the $x_{\rm vis}$ distribution is peaked at small x and falls rapidly to zero by $x_{\rm vis} \simeq 0.7$. Again there are no events above $x_{\rm vis}=1$. The $y_{\rm vis}$ distribution follows a curve which peaks at $y_{\rm vis} \simeq 0.8$. This is again a good signal for the leptonic cascade process.

The comments in Sec. IV concerning the changes caused by switching to light-to-heavy quark transitions, different mass assignments, $V+A$ couplings and antineutrino reactions producing $\mu^+\mu^+$ events are generally valid here. In Fig. 21 we show the $E_{\rm had}$, $E_{\rm vis}$, and $E_{\rm tot}$ distributions for the light-to-heavy quark transition. The hadronic energy

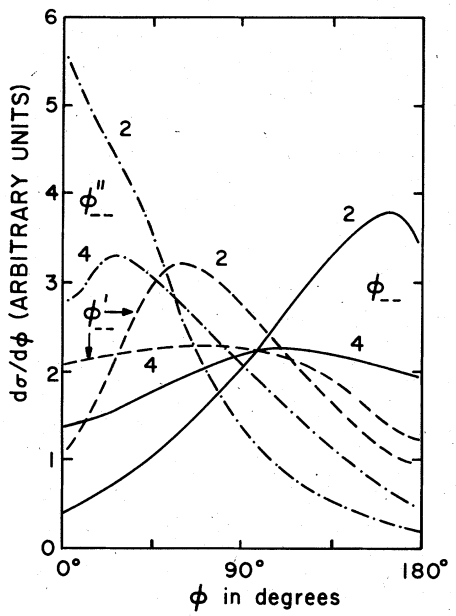

FIG. 29. The distributions in the azimuthal opening angles ϕ_{--}, ϕ'_{--}, and ϕ''_{--}. The curves marked 2 and 4 refer to $m_L=2$ GeV/c^2 and $m_L=4$ GeV/c^2, respectively.

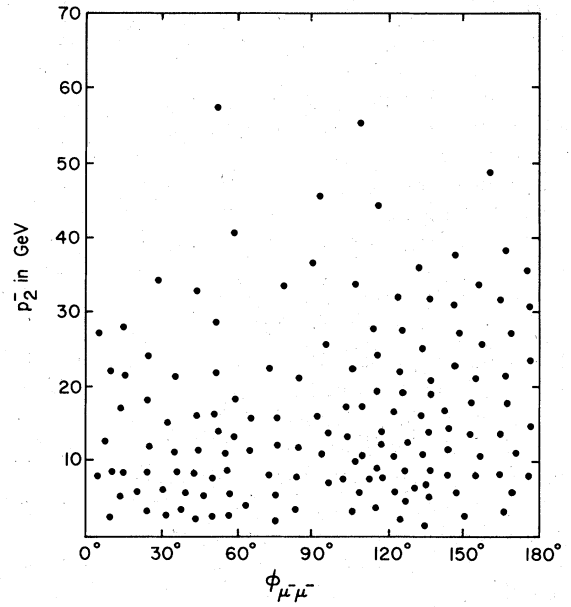

FIG. 30. Scatter plot of ϕ_{--} versus p_2^-.

threshold is pushed to a larger value, again the z distributions peak at slightly lower values. In Fig. 26 we show the $M_{\rm had}$ distribution for the light-to-heavy quark transition. The $x_{\rm vis}$ and $y_{\rm vis}$ distributions change also to make $x_{\rm vis}$ peak for small-

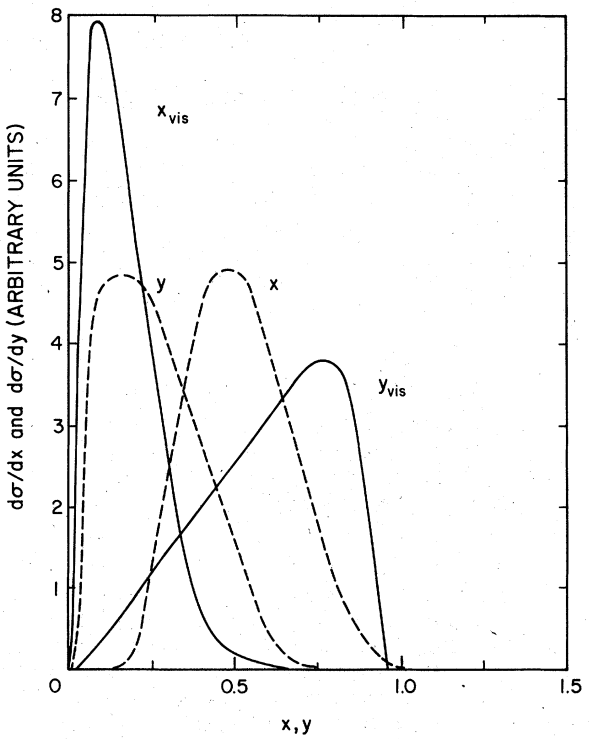

FIG. 31. The distributions in x,y for the M^- production and $x_{\rm vis}$ and $y_{\rm vis}$ defined with respect to the fast μ^-.

er x and y_{vis} peak for larger y. One of the most sensitive variables to the L^0 mass is the ϕ angle between the two muons. As we lower the L^0 mass, ϕ_{--} peaks nearer 180°, ϕ''_{--} peaks near 0°, and ϕ'_{--} develops a maximum in the region near 50°. We have shown these changes in Fig. 29. The reason for the peaking of ϕ_{--} near 180° is that the light L^0 balances the μ^- (and $\bar{\nu}_\mu$) transverse momenta when the M^- decays, and when L^0 subsequently decays the second μ^- transverse momentum will be small.

VI. TRIMUON EVENTS

The trimuon events in our model come from the decay chain depicted in Fig. 4. Branching ratios have already been discussed in Sec. III. As far as the distributions are concerned, we fold the M^- polarization vector with the expression for polarized M^- decay given in Eq. (5.1) and then add the leptonic decay of an unpolarized L^0 particle. This part of the calculation was also done by taking the trace on the M^- line and using the narrow-width approximation so that we have two independent checks on our answers. As in Sec. V. we distinguish between the two identical μ^- particles by ordering them in the Monte Carlo calculation into $\mu_1 \equiv \mu^-_{\text{fast}}$ and $\mu_2 \equiv \mu^-_{\text{slow}}$. For convenience we call $\mu_3 \equiv \mu^+$. We have folded the neutrino flux for quadrupole-triplet focusing with the distributions. We have already published some of the trimuon distributions at $E = 200$ GeV. in Ref. 9.

In Fig. 32 we plot the differential spectra in the energies of the muons, the missing energy, the energy of the hadrons, the visible energy, and the total energy. The distribution in E_{vis} peaks near 150 GeV and has a long tail which stretches out to the end point of the neutrino spectrum. The presence of two unobservable neutrinos now pushes the peak in the hadronic energy to a lower value. The spectra in the parameters $z_1^- = E_1^-/E_{\text{vis}}$, $z_2^- = E_2^-/E_{\text{vis}}$, and $z_3^+ = E_3^+/E_{\text{vis}}$ are then shown in Fig. 33. These spectra are peaked for low values of the z variables. The analogous z' variables for the slow μ^- and μ^+ are flatter. We then give the scatter plot of p_2 versus p_3 in Fig. 34. All these distributions show the same characteristics as in those seen previously for the $\mu^-\mu^+$ and $\mu^-\mu^-$ events, leading us to expect a rather large contamination of dimuon events by misidentified trimuon events. The detection efficiency for multimuons is needed before accurate numbers can be given for event rates into these channels.

The spectra in the opening angles between the muons are given in Fig. 35. The polar-angle distributions with respect to the neutrino beam direction are similar to those shown previously so we see no need to repeat them. Note that all these angles are very small. Two-dimensional scatter plots of opening anges were given in Ref. 9, where we showed the difference between the unordered

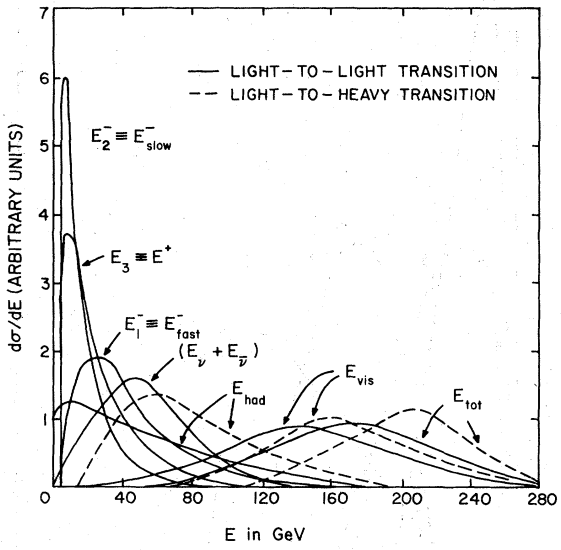

FIG. 32. The energy distributions for the fast μ^-, the slow μ^-, the μ^+, the missing energy $E_\nu + E_{\bar{\nu}}$, the hadronic energy E_{had}, the visible energy E_{vis} and the total energy E_{tot}, all flux-averaged with the quadrupole-triplet spectrum. The solid curves refer to light-to-light quark transitions while the dashed curves refer to light-to-heavy quark transitions.

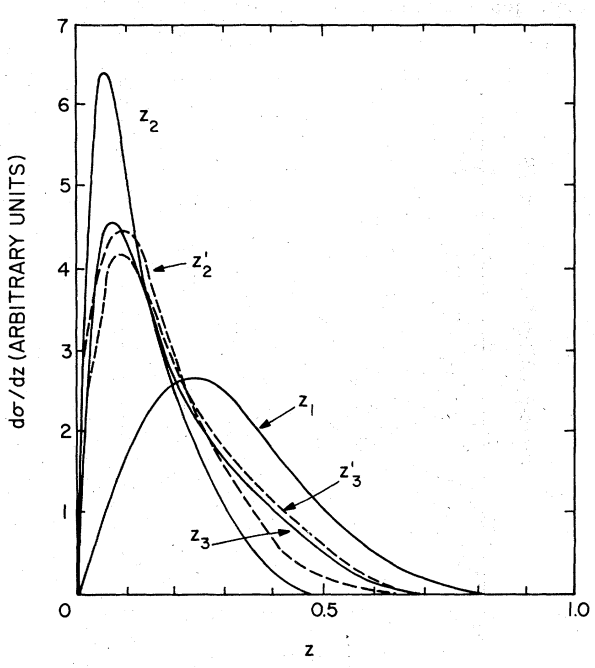

FIG. 33. The distributions in $z_1 = E_1/E_{\text{vis}}$, $z_2 = E_2/E_{\text{vis}}$, $z_3 = E_3/E_{\text{vis}}$, $z'_2 = E_2/(E_{\text{vis}} - E_1)$, and $z'_3 = E_3/(E_{\text{vis}} - E_1)$.

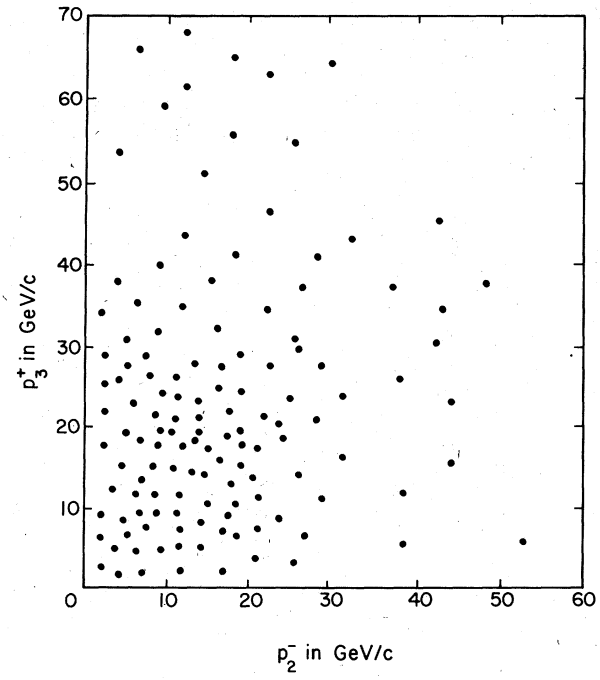

FIG. 34. The scatter plot of p_2 versus p_3.

and ordered μ^- particles (with respect to the energy). These plots are again similar to those given in the previous sections.

The invariant-mass distributions of the muons and hadrons is shown next in Figs. 36 and 37. M_{123} is the total invariant mass of the three muons and peaks at approximately one-half the mass of the M^- particle. The invariant masses of the two-particle combinations M_{12}, M_{23}, and M_{13} all peak at approximately one half the mass of the L^0. Note that M_{23} does extend above 4 GeV/c^2 because some of the slow μ^- actually come from the M^- decay. Figure 36 gives results for $m_M = 8$ GeV/c^2 and m_L

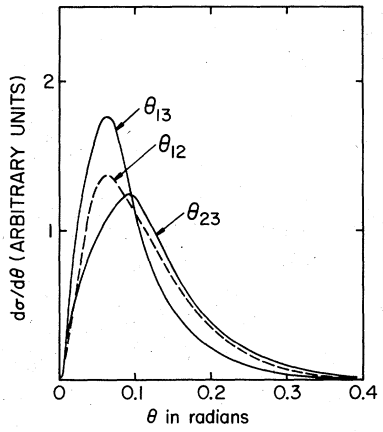

FIG. 35. The relative opening angles between the muons.

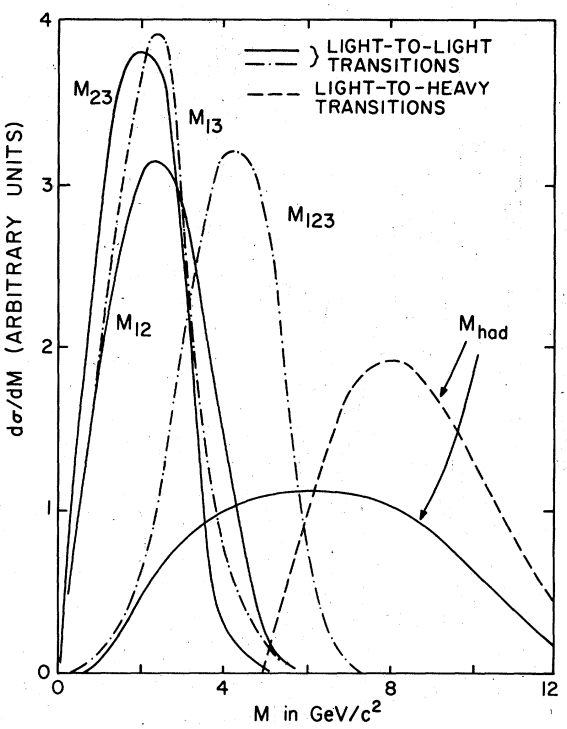

FIG. 36. The invariant masses of the muons and the hadrons for $m_M = 8$ GeV/c^2 and $m_L = 4$ GeV/c^2. The solid and dot-dashed curves refer to light-to-light quark transitions while the dashed curve refers to light-to-heavy quark transitions.

= 4 GeV/c^2 with light-to-light quark transitions. Figure 37 shows the same results for $m_M = 8$ GeV/c^2 and $m_L = 2$ GeV/c^2. Then we give the plots in the rapidities, the rapidity sum and various rapidity differences, in Fig. 38. The peaks in the rapidities are between $Y = 2.5$ and 4.0, while the rapidity differences range from -0.2 to $+1.0$.

We now present the distributions in the transverse momenta of the muons. These are given in Fig. 39 for the projections onto the different (x, y) planes. The average $p_\perp$ increases dramatically as we go from $p_\perp$ to $p'_\perp$ to $p''_\perp$. In fact, transverse momenta as large as 6 GeV/c are characteristic for $p''_\perp$. Such momenta will not be so large in the case of heavy hadronic decay processes because the masses involved are in the range of 2–3 GeV/c^2 rather than the 8 GeV/c^2 we assume for the M^- mass.

The angles between the muon momentum vectors projected onto the (x, y) planes will be a crucial test of this type of model. We show in Fig. 40 the distributions on the (x, y) plane for ϕ_{12}, ϕ_{13}, and ϕ_{23}, and also the distributions in the same variables projected on the (x', y') and (x'', y'') planes. We have also chosen other combinations, such as the angle between the resultant of the $\mu_2\mu_3$ vectors

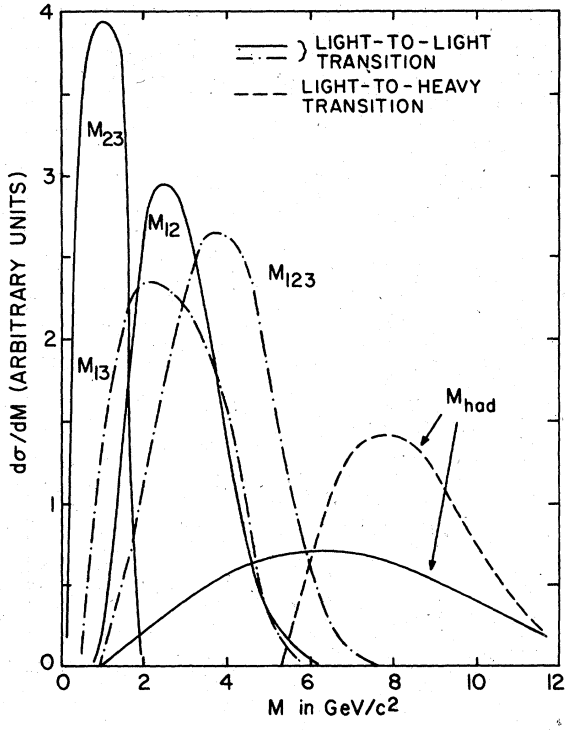

FIG. 37. The invariant masses of the muons and the hadrons for $m_M = 8$ GeV/c^2 and $m_L = 2$ GeV/c^2. The solid and dot-dashed curves refer to light-to-light quark transitions while the dashed curve refers to light-to-heavy quark transitions.

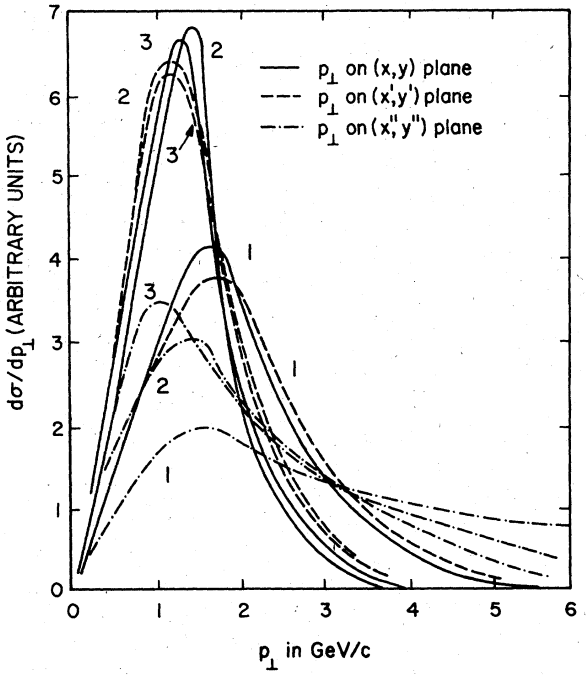

FIG. 39. The spectra in the muon transverse momenta (1, 2, and 3 refer to μ_1, μ_2, and μ_3, respectively).

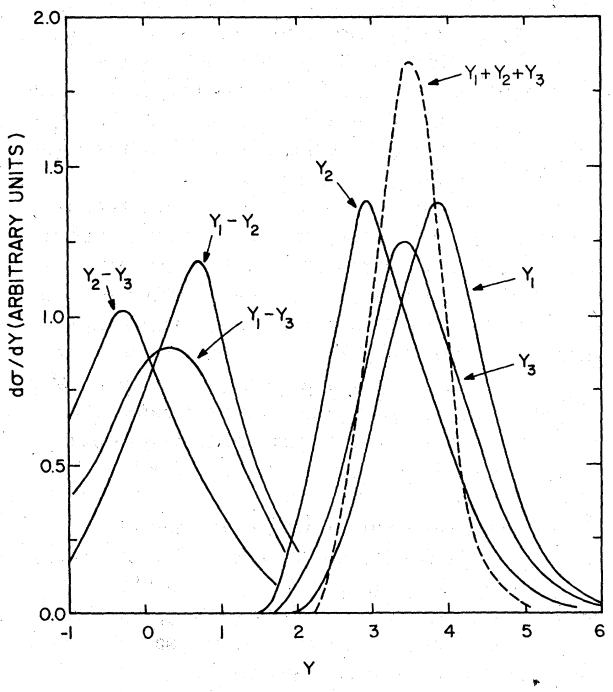

FIG. 38. Rapidity plots for μ_1, μ_2, μ_3, the rapidity sum, and the rapidity differences.

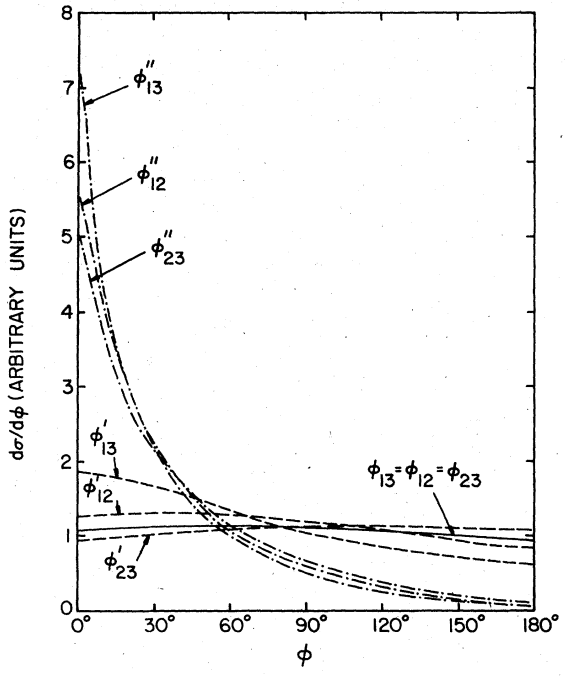

FIG. 40. The spectra in the angles $\phi_{12}, \phi_{13}, \phi_{23}$, etc. The notation is explained in the text.

with respect to the μ_1 vector, which is denoted by $\phi_{1(2,3)}$. Some of these plots were already given in Ref. 9 for a beam energy of 200 GeV. For completeness we give all of them in Fig. 41. We see very clearly the peaking towards zero degrees between the projections on the (x', y') and (x'', y'') planes. This reflects the result of our model that all the muons tend to lie on one side of the W-boson direction. Such a phenomenon is certainly not expected from heavy-charmed-particle decays. The flat distributions in the (x, y) plane indicate almost zero correlation between the vectors projected perpendicular to the neutrino direction. This direction is equivalent to the M^- direction because the heavy particle tends to go along the z axis. We have computed the ϕ''_{12}, ϕ''_{13}, and ϕ''_{23} values for the three completely measured trimuon events observed by the FHPRW group. They all have low values below 90° consistent with this interpretation. Obviously, the correlations between the ϕ angles will be the key to distinguishing between different production models.

Finally, we give the distributions in x, y for the M^- and $x_{\rm vis}$, $y_{\rm vis}$ defined with respect to the fast μ^- in Fig. 42. Note that the distribution in $x_{\rm vis}$ has a maximum below that of x and also has a long tail extending above unity, while y peaks at a value larger than the value of the peak in y. The $y_{\rm vis}$ distribution does not peak at such a large y as in the previous sections.

We have also examined the effects of changing the quark and lepton masses. In Fig. 32 we show the energy distributions for the light-to-heavy quark transitions. The most dramatic change now occurs in $E_{\rm had}$ which must have a large threshold. The actual value of this threshold is determined by

$$E_{\rm th,had} = (W_{\rm th}^2 + q_{\rm min}^2 - M^2)/2M\,.$$

For the cases we have illustrated where a light quark converts into a heavy quark with mass 4 GeV/c^2 and with $W_{\rm th}$=5 GeV, this implies that $E_{\rm had} \simeq 15$ GeV when we flux average. We give this value explicitly because trimuon event number 119 of the FHPRW group has a hadronic energy of only 13 ±2 GeV. As we mentioned previously[9] this event has a relatively low probability in the light-to-light quark transition and becomes problematic in the light-to-heavy case.[30] It will be very interesting to see whether more events of this type can be found. We note that the $E_{\rm vis}$ and $E_{\rm tot}$ curves in Fig. 32 are also pushed to higher energies.

As we noted previously, the changes in the muon distributions are rather small, and move the peaks in the z variables to lower values. We remark here that the z distributions fall to zero because we have a cut on the muon energies. In Figs. 36 and 37 we show the changes in the $M_{\rm had}$ distribution

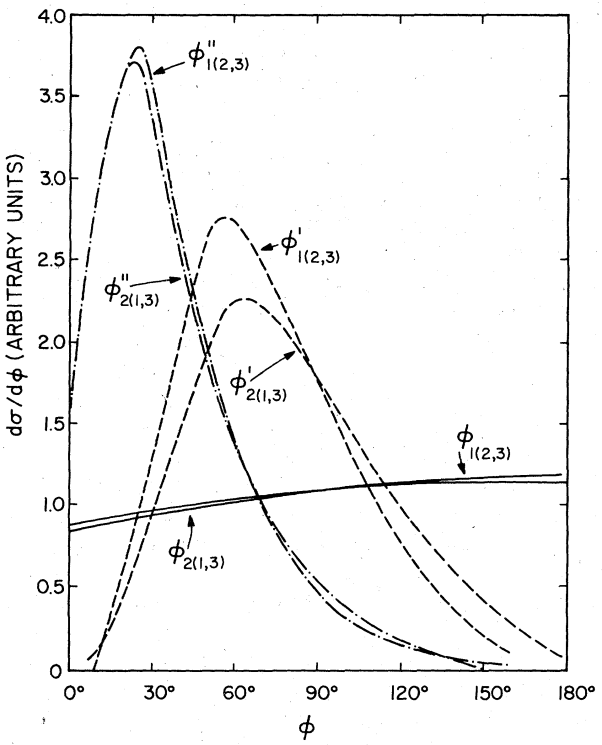

FIG. 41. The spectra in the angles $\phi_{1(2,3)}$, $\phi_{2(1,3)}$ etc. The notation is explained in the text.

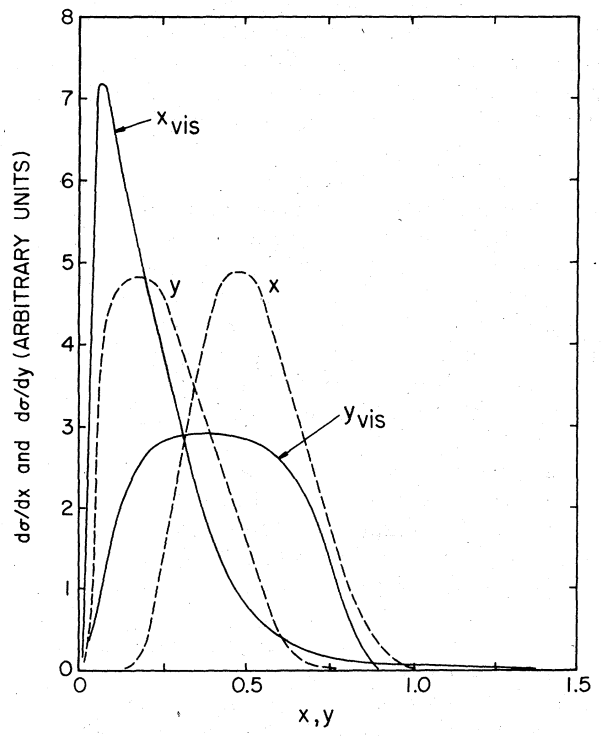

FIG. 42. The distributions in x, y for M^- production and $x_{\rm vis}$, $y_{\rm vis}$ defined with respect to the fast μ^-.

which now has a threshold at 5 GeV/c^2. The x_{vis} plot now peaks nearer to $x=0$ while the y_{vis} plot peaks nearer $y=1$.

The effects of changing the L^0 mass are documented in Figs. 36 and 37 where we show the changes in M_{12}, M_{23}, M_{13}, and M_{123}. The φ distributions become peaked towards zero degrees as we lower the L^0 mass. These effects are very similar to those shown in Fig. 18 so we do not need to repeat them.

VII. CONCLUSIONS

In the previous sections we have exhaustively examined the $\mu^-\mu^+$, $\mu^-\mu^-$, and $\mu^-\mu^-\mu^+$ event rates and distributions expected from a typical heavy-lepton cascade chain. The present small data sample of trimuon and same-sign dimuon events have the characteristics expected from such a process. Clearly an increase in data is needed before definite conclusions can be drawn.

The event rate predicted on the basis of reasonable heavy-lepton masses and decay branching ratios is so close to the uncorrected experimental number that it leaves little room for a large mixing angle at the M^- production vertex.[9] If this situation remains unchanged then one reasonable conclusion is that the new leptons have to be assigned to the same gauge-group representation as the ν_μ and the μ^-. We therefore are led to believe that gauge groups larger than SU(2)$\times$U(1) will be required to fit the trimuon events. The possibility of new gauge-field couplings involving heavier quarks has been investigated and the production rate is not suppressed enough to cause any problem. The heavy-lepton masses can be adjusted to partially close some decay channels and allow larger branching ratios into leptonic modes. The net effect of both changes is to lead to roughly comparable event rates. Other authors[10] have taken a different interpretation of the leptonic-cascade model, namely, that mixing angles are possible and the SU(2)$\times$U(1) model still fits the data. Time will tell.

The ratio of antineutrino-induced $\mu^+\mu^-$, $\mu^+\mu^+$, $\mu^+\mu^+\mu^-$ events to neutrino induced $\mu^-\mu^+$, $\mu^-\mu^-$, $\mu^-\mu^-\mu^+$ events is expected to be small because the event rate is very sensitive to the high mass threshold and the antineutrino flux falls much faster than the neutrino flux. If we use only light-to-light quark transitions then we estimate a ratio of 3% between antineutrino and neutrino event rates for the FHPRW experiment. This number can be as large as 17% in the case of light-to-heavy quark transitions with $V+A$ couplings.

The distributions are basically determined by the kinematics of the cascade chain. When a heavy lepton with a mass of approximately 8 GeV/c^2 is produced it goes primarily along the beam direction. When the L^0 mass is relatively heavy it too goes mainly in the z direction. The decay muons are then emitted at uncorrelated azimuthal angles with respect to the neutrino beam. In particular the angles between the muon vectors projected on the (x, y) plane are relatively flat. However, if we decrease the L^0 mass the second muon (or muon pair) cannot have such a large $p_\perp$ value with respect to the L^0 direction so they tend to come out at 180° with respect to the initial muon. As we move to the different (fictitious) W-boson axes, the spray of muons all tend to be on one side of these axes so the distributions in the opening angles in the (x', y') and (x'', y'') planes tend to peak dramatically at small angles. We hope that this feature will be useful in determining the L^0 mass as well as distinguishing between our model and hadronic interpretations of the data.

The production of charmed particles via the standard valence and sea distributions leads to completely different results.[12] Models based on the production of heavy quarks, which decay through lighter quarks and lead to $\mu^-\mu^-\mu^+$ events, can be expected to have the same features. The fact that there is a hadronic jet always leads to a strong correlation near $\phi=180°$ between the fast-μ^- momentum vector and the resultant formed from the two slow muons. Even with the currently small data sample there is no evidence for such a correlation. A diffractive production model[13] may lead to distributions similar to ours because the hadrons are produced at small x_{vis} and all decay particles go in the forward direction. We anticipate that the different $p_\perp$ distributions will be crucial here. The leptonic-cascade interpretation can lead to large $p_\perp$ values whereas the diffractive model, because the masses involved are smaller, should not give events with large transverse momenta. We hope that antineutrino results will distinguish between the models also, because we are very sensitive to the energy threshhold whereas the diffractive model is not.

In those events where the hadron energy is measured the x_{vis} and y_{vis} distributions will be very illuminating. The fact that the y_{vis} distribution peaks for large y_{vis}, especially in the $\mu^-\mu^+$ and $\mu^-\mu^-$ events, gives a good signal. Whether one can exploit these distributions to extract heavy-lepton signals from the regular μ^- inclusive scattering is a nontrivial but important question, which is currently under investigation. The acceptance, resolution, and detection efficiency of the experimental apparatus are crucial here.

The fact that the kinematics rather than the dynamics determines the key distributions means

that they will be of little importance in distinguishing between gauge-theory models, other than setting threshold values for masses. One must therefore confront all models with the *corrected* event rate which can be compared with the theoretical production cross section times branching ratios. The latter numbers vary widely from model to model. Those models which have heavy quarks produced together with heavy leptons are interesting in their own right because they could lead to events with four or more muons. Unfortunately all the muons have energy distributions which peak at low energies. We already lose one-third of our event rate for trimuons with the low-energy cut of 4 GeV on each muon energy. The effect of a cut becomes more serious as we increase the number of muons. The existence of events with more muons will hopefully resolve itself once more data are available.

To conclude we reiterate that the trimuon events as well as the same-sign dimuon events can be fit by a heavy-lepton cascade model but with rates which seem to imply the existence of a larger gauge group for the weak and electromagnetic interactions.

ACKNOWLEDGMENTS

We have benefited greatly from discussions with the members of the FHPRW group, especially with A. K. Mann and D. Cline. We would also like to acknowledge useful conversations with B. W. Lee, H-T. Nieh, C. Quigg, and R. Shrock. J. Smith would also like to thank Fermilab for hospitality.

---

*Work supported in part by the National Science Foundation under Grants Nos. PHY-75-05467 A01 and PHY-76-15328.

†Permanent address.

[1]Y-S Tsai, Phys. Rev. D 4, 2821 (1971); J. D. Bjorken and C. H. Llewellyn Smith, Phys. Rev. D 7, 887 (1973). References to early speculation on the existence of heavy leptons including gauge-theory classifications can be traced from the following review articles: M. L. Perl and P. Rapidus, SLAC Report No. SLAC-PUB-1496, 1974 (unpublished); C. H. Albright, C. Jarskog, and M. O. Tjia, Nucl. Phys. B86, 535 (1975); A. S. Goldhaber and J. Smith, Rep. Prog. in Phys. 38, 371 (1975); C. H. Llewellyn Smith, Proc. R. Soc. (to be published).

[2]M. L. Perl *et al.*, Phys. Rev. Lett. 35, 1489 (1975); Phys. Lett. 63B, 466 (1976).

[3]R. Felst, invited talk at the Chicago APS meeting, 1977 (unpublished).

[4]B. C. Barish, *et al.*, Phys. Rev. Lett. 31, 180 (1973); 32, 1387 (1974); see also B. C. Barish in *Proceedings of the Sixth Hawaii Topical Conference on Particle Physics*, edited by P. N. Dobson, Jr., S. Pakvasa, U. Z. Peterson, and S. F. Tuan (Univ. of Hawaii, Honolulu, 1975).

[5]A. Benvenuti, *et al.*, Phys. Rev. Lett. 35, 1199 (1975); 35, 1203 (1975); 35, 1249 (1975); B. C. Barish, *et al.*, *ibid.* 36, 939 (1976); and A. Bodek, in Proceedings of the Summer Institute on Particle Physics, SLAC, 1975 (unpublished).

[6]L. N. Chang, E. Derman, and J. N. Ng, Phys. Rev. Lett. 35, 6 (1975); Phys. Rev. D 12, 3539 (1975); C. H. Albright, Phys. Rev. D 12, 1319 (1975); A. Pais, and S. B. Treiman, Phys. Rev. Lett. 35, 1206 (1975).

[7]B. C. Barish, *et al.*, Phys. Rev. Lett. 38, 577 (1977); A. Benvenuti, *et al.*, Phys. Rev. Lett. 38, 1110 (1977); D. Cline, in *Particles and Fields '76*, Proceedings of Annual Meeting of the Division of Particles and Fields of the APS, Brookhaven National Laboratory, edited by H. Gordon and R. F. Peierls (BNL, Upton, New York, 1977), p. D37; O. Fackler, *ibid.*, p. C53.

[8]T. P. Cheng and L.-F. Li, Phys. Rev. Lett. 38, 8 (1977); see also talk at *Orbis Scientiae*, Coral Gables, Florida, 1977 (unpublished); Phys. Rev. D 16, 1425 (1977). S. M. Bilenky, S. T. Petcov, and B. Pontecorvo, Phys. Lett. 67B, 309 (1977); S. M. Bilenky and S. T. Petcov (unpublished); F. Wilczek and A. Zee, Phys. Rev. Lett. 38, 531 (1977); B. W. Lee, S. Pakvasa, R. E. Shrock, and H. Sugawara, Phys. Rev. Lett. 38, 937 (1977); H. T. Nieh, Phys. Rev. D 15, 3413 (1977); J. D. Bjorken, K. Lane, and S. Weinberg, *ibid.* 16, 1474 (1977); S. B. Treiman, F. Wilczek, and A. Zee, *ibid.* 16, 153 (1977); W. J. Marciano and A. I. Sanda, Phys. Rev. Lett. 38, 1512 (1977); V. Barger and D. V. Nanopoulos, Nucl. Phys. (to be published); B. W. Lee and R. E. Shrock, Phys. Rev. D 16, 1444 (1977).

[9]C. H. Albright, J. Smith, and J. A. M. Vermaseren, Phys. Rev. Lett. 38, 1187 (1977).

[10]V. Barger, T. Gottschalk, D. V. Nanopoulos, J. Abad, and R. J. N. Phillips, Phys. Rev. Lett. 38, 1190 (1977).

[11]P. Langacker and G. Segrè, Phys. Rev. Lett. 39, 259 (1977); B. W. Lee and S. Weinberg, Phys. Rev. Lett. 38, 1237 (1977).

[12]A. Benvenuti *et al.*, Phys. Rev. Lett. 38, 1183 (1977).

[13]F. Bletzacker, H. T. Nieh, and A. Soni, Phys. Rev. Lett. 38, 1241 (1977).

[14]C. H. Albright, Phys. Rev. Lett. 28, 1150 (1972); Phys. Rev. D 7, 63 (1973); A. Soni, Phys. Rev. D 9, 2092 (1974); 11, 624 (1975). The production of positively charged leptons by neutrino beams has been studied by C. H. Albright and C. Jarlskog, Nucl. Phys. B84, 467 (1975); C. H. Albright, C. Jarlskog, and L. Wolfenstein, Nucl. Phys. B84, 493 (1975).

[15]H. Georgi and H. D. Politzer, Phys. Rev. Lett. 36, 1281 (1976); Phys. Rev. D 14, 1829 (1976); A. De Rújula, H. Georgi, and H. D. Politzer, Ann. of Phys. (N.Y.) 103, 315 (1977); O. Nachtmann, Nucl. Phys. B63, 237 (1973); *ibid.* B78, 455 (1974); V. Baluni and E. Eichten, Phys. Rev. Lett. 37, 1181 (1976); R. Barbieri, J. Ellis, M. K. Gaillard, and G. G. Ross, Nucl. Phys. B117, 50 (1976); R. Ellis, R. Petronzio, and G. Parisi, Phys. Lett. 64B, 97 (1976); D. J. Gross,

S. B. Treiman, and F. A. Wilczek, Phys. Rev. D 15, 2486 (1977).
[16]O. Nachtmann, see Ref. 15.
[17]C. G. Callan and D. J. Gross, Phys. Rev. Lett. 22, 156 (1969).
[19]D. J. Gross and C. H. Llewellyn Smith, Nucl. Phys. B14, 337 (1969).
[19]C. H. Albright and C. Jarlskog, see Ref. 14.
[20]S. Pakvasa, D. Parashar, and S. F. Tuan, Phys. Rev. D 10, 2124 (1974).
[21]C. H. Llewellyn Smith, Phys. Rep. 3C, 261 (1972).
[22]C. H. Albright and R. E. Shrock, Phys. Rev. D 16, 575 (1977).
[23]C. H. Albright, Phys. Rev. D 13, 2508 (1976); see also K. Ishikawa, S. Midorikawa, and M. Yoshimura, report No. TU/77/61 (unpublished).
[24]We note that coupling strengths in gauge models could make the decays (3.1e)–(3.1h) actually larger than their (3.1a)–(3.1d) counterparts. Our assertion is only true for equal coupling constants. In specific models such as the SU(3)⊗U(1) models of Lee and Weinberg, and Langacker and Segrè (see Ref. 11), the decay $M \to \nu_\mu \bar{L}^0 \mu^-$ is allowed with comparable strength to the decay $M^- \to L^0 + \mu^- + \bar{\nu}_\mu$. We have investigated this alternate decay chain and computed the resultant trimuon energy distributions. For the masses and couplings chosen in the paper we find very similar distributions to the ones given. Hence this extra decay mode only changes the trimuon branching ratio. We have chosen not to complicate our figures by adding the other distributions.
[25]T. Ling, invited talk at the Washington APS meeting, April 1977 (unpublished). See also V. Barger *et al.*, Wisconsin Report No. COO-603 (unpublished).
[26]L. M. Sehgal and P. Zerwas, Phys. Rev. Lett. 36, 399 (1976); Nucl. Phys. B108, 493 (1976); V. Barger and R. J. N. Phillips, Phys. Rev. D 14, 80 (1976).
[27]For experimental results see the talk by R. F. Schwitters in *Proceedings of the 1975 International Symposium on Lepton and Photon Interactions at High Energies, Stanford, California,* edited by W. T. Kirk, (SLAC, Stanford, 1976).
[28]We require the value of $R(s)$ below $\sqrt{s} \simeq 4$ GeV. Therefore we are justified in neglecting the heavy-lepton contribution to $R(s)$ because, for $m_\tau = 1.9$ GeV/c^2 we are effectively below the threshold for heavy-lepton pair production and below the threshold for charmed-particle production.
[29]We have investigated the production of M^- in two cases: (1) neglecting spin effects and (2) including spin effects completely. The resulting difference in the cross section is very small, of the order of a few percent. Note that the M^- polarization is relatively large near threshold. However, we always fold the cross section with the neutrino spectrum which averages out such effects. Because the M^- polarization is so small, we expect the massive L^0 to possess an even smaller polarization which can be safely neglected. For completeness we have also investigated the consequences of changing the couplings at the $M^- \to L^0$ vertex and at the $L^0 \to \mu^-$ vertex. The differences between choosing $V-A$ and $V+A$ couplings were always less than 10%, reflecting the fact that the kinematics rather than the dynamics determine the trimuon distributions.
[30]This assumes that all the hadronic energy is visible. In a certain class of models, such as proposed by Lee and Weinberg (Ref. 11), part of the energy released when the heavy quark changes to a light quark is emitted as leptonic energy.